HEP'97 #306
Submitted to Pa 17
Pl 13

DELPHI 97-121 CONF 103
20 July, 1997

The Silicon Tracker in the DELPHI Experiment at LEP2

Preliminary

DELPHI Collaboration

The Silicon Tracker Group

Bratislava, CERN, Grenoble, Helsinki, Karlsruhe, Kraków, Ljubljana, CPPM Marseille, Milano, LAL Orsay, Oxford, Padova, CdF Paris, LPNHE Paris, Prague, RAL, Roma, Santander, Uppsala, Vienna, Wuppertal

Abstract

The final upgrade of the DELPHI Silicon Tracker, to enable DELPHI to meet the physics requirements of LEP2, was completed in 1997. The tracker contains 888 detecting elements having a total active surface of about 1.6 m^2 of silicon, has 1399808 readout channels and covers polar angles between 11° and 169°. It consists of: the Silicon Barrel, extending from 21° to 159° and playing the role of vertex detector and the Very Forward Tracker (VFT) in the form of two silicon endcaps, providing standalone pattern recognition and increasing the track reconstruction efficiency between 11° and 25°. The complete Silicon Barrel and a large part of the VFT was already in operation during the 1996 data taking at LEP2. The complete Silicon Tracker is now installed and is currently taking data. The Silicon Barrel consists of 640 AC coupled microstrip silicon detectors, arranged in three layers at average radii of 6.3, 8.9 and 10.8 cm. The 149504 electronics channels read signals collected on the strips which give either $R\phi$ measurements (in all three layers, with a readout pitch of 50 μm) or Rz measurements (in two and a half layers, with a readout pitch between 42 μm and 176 μm). The material in the sensitive region is kept to a minimum by the use of double sided detectors, double metal readout and light mechanics. Each of the two VFT endcaps contains two layers of silicon pixel detectors and two layers of ministrip detectors. The pixels (squares of 330 $\times$ 330 μm^2, 1225728 in total) are connected to the readout electronics channels using an industrial bump bonding method. Their readout is performed by a sparse data scan circuit. The AC coupled ministrip detectors (96 in total) have a strip pitch of 100 μm, a readout pitch of 200 μm and a signal to noise ratio of about 40. DELPHI is one of the first experiments in which the pixel detectors are used in tracking.

Paper submitted to the HEP'97 Conference
Jerusalem, August 19-26

1 Introduction

The DELPHI Silicon Tracker presented in this paper has been optimized to cope with the requirements posed by the physics programme at LEP2. The design [1] had to take into account the following features of the processes studied or searched for:

- Four fermion processes, important for both standard and non-standard physics, are relatively frequent, hence a larger angular coverage in θ [1] is required compared to Z° physics.
- The search for the light Higgs boson and for supersymmetric particles is one of the most important physics objectives for LEP2, so a good tagging of b quarks down to low θ angles is important in order to reduce background from the standard processes like WW production.
- In the processes with the largest cross sections, such as $e^+e^- \to q\bar{q}\gamma$ or $e^+e^- \to \gamma\gamma$, the particles are produced predominantly at lower values of θ.

The design of the Silicon Tracker had then two objectives:

- Building up a central vertex detector of the same quality as the previous vertex detector [2] but with b-tagging capability down to $\theta \approx 25^\circ$. This is realized with three layers of silicon microstrip detectors, measuring the $R\phi$ and Rz coordinates and with the material in the sensitive region kept to minimum. This part is called the Silicon Barrel.
- The improvement of tracking down to 11° in θ by adding endcaps made of silicon providing a standalone pattern recognition in the very forward region of DELPHI. As opposed to the Barrel, a spatial resolution of the track measurements of the order of 100 μm is sufficient. Such a detector gives an improvement of the hermeticity and a better extrapolation of tracks towards the forward RICH detectors, leading to a better particle identification in this region, e.g. for a study of exclusive processes in two-photon interactions. The endcaps contain two layers of Pixel detectors and two layers of the Ministrip detectors. This part is called the Very Forward Tracker (VFT).

To make the project affordable various components and systems have been reused from the previous silicon vertex detectors of DELPHI, namely some of the plaquettes and hybrids [2] and the data acquisition and service systems [3]. The complete Silicon Barrel and a large part of the VFT (the full set of Ministrip detectors and 60% of the Pixels) was in operation during the 1996 data taking. The complete detector was installed in DELPHI for the data taking in 1997. As an illustration of its physics capabilities we show in fig. 1 an event registered in 1996 at the energy $\sqrt{s} = 161$ GeV/c^2, where a jet with $\theta = 35^\circ$ is tagged as a b jet.

[1] In the standard DELPHI coordinate system, the z axis is along the electron direction, the x axis points towards the center of LEP, and the y axis points upwards. The polar angle to the z axis is called θ and the azimuthal angle around the z axis is called ϕ; the radial coordinate is $R = \sqrt{x^2 + y^2}$.

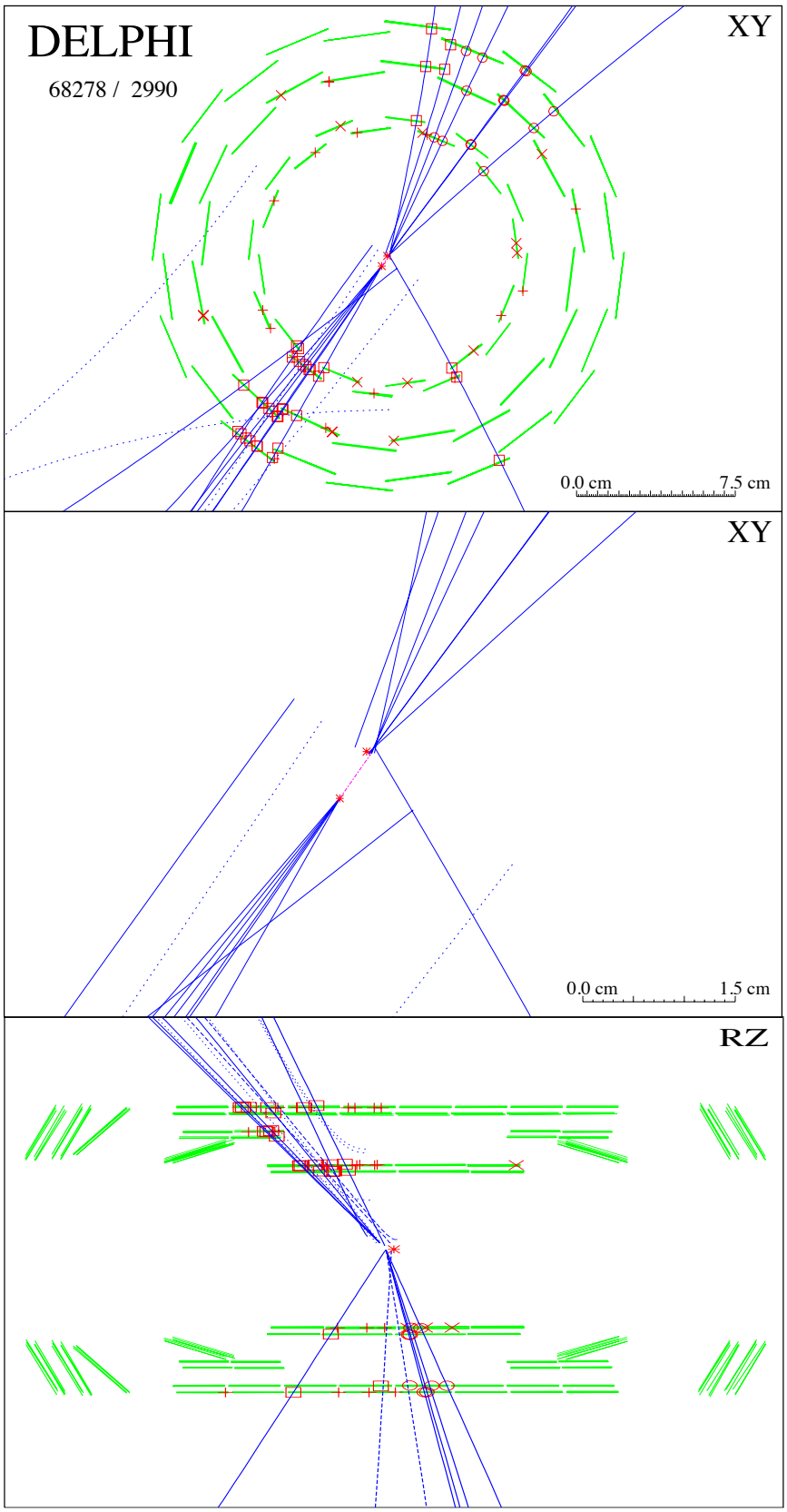

Figure 1: Event registered during the 161 GeV/c^2 run. The top two views show the $R\phi$ projection on two different scales. The displaced vertex is clearly seen. The bottom view displays the Rz projection, showing that the b jet is tagged at $\theta = 35°$.

2 Design Considerations

The Silicon Tracker uses different kinds of technologies in each angular region in order to achieve the performance goals discussed above. Each track passing through the detector gives between 2 and 6 three dimensional measurements, with varying resolution. In the barrel region the b-tagging performance must be equivalent to that of the previous detector, and in addition be extended down to around 25°, beyond which multiple scattering starts to dominate the impact parameter resolution for B hadron decay products. This is achieved with three layers of microstrip modules, termed Closer, Inner and Outer, giving between 3 and 6 hits per track. In the $R\phi$ plane the resolution is around 8 μm, and in the Rz plane the readout pitch is changed for plaquettes at different angles to give the best resolution possible perpendicular to the track, varying between about 10 μm for vertical tracks and 20 μm for the most inclined tracks. In the forward region, the emphasis is on standalone pattern recognition and momentum measurement. The momentum measurement is limited by Coulomb scattering and a resolution of about 100 μm is sufficient. This gives an angular accuracy of about 1 mrad, and tracks are extrapolated with a resolution of a few mm towards the forward tracking chambers of DELPHI. Simulation studies [1] have shown that with four planes of detectors, the optimal performance is given by two planes of back to back ministrip detectors, with a readout pitch of 200 μm, and two planes of pixel detectors, crucial to eliminate ghost tracks, of 330×330 μm^2.

Throughout the detector there is great emphasis on the overlap of sensitive silicon, within each plane of detectors, and between the different planes. This provides redundancy and makes possible a self alignment procedure, but places great constraints on the assembly, with silicon plaquettes from different layers often lying less than 1mm apart.

The Silicon Tracker is illustrated in figure 2. The three concentric layers of the barrel detector cover the angular region $21° - 159°$. Two pixel planes, the first one being located inside the barrel, and two ministrip detector endcaps cover the angular region $11° - 26°$ and $154° - 169°$. Full technical descriptions of the detector and the individual layers can be found in [4]- [8]. In what follows we give a summary only, mentioning in particular the new features.

3 Silicon Components

The characteristics of the silicon plaquettes used are summarised in table 1. The wafers are n-type silicon, approximately 300 μm thick, with operational voltages ranging from about 40-60V for the single sided devices, to 95V for full depletion of some double-sided detectors. The suppliers used were Hamamatsu [2], SINTEF [3] , CSEM [4] and MICRON [5].

For the first measured point in the barrel, where multiple scattering is crucial, double-sided detectors are used. The layer is taken from the previous detector [2]. The angular resolution of tracks is dominated by the silicon detector and hence the multiple scattering on the outermost point does not worsen the impact parameter resolution. Hence, the cheaper back-to-back solution is chosen for the Outer layer. This layer is completely

[2]Hamamatsu Photonics K.K., Hamamatsu City, Japan
[3]SINTEF, Oslo, Norway
[4]CSEM,Rue de la Maladiére 41, CH 2007, Neuchatel, Switzerland
[5]MICRON Semiconductor Limited, Sussex BN15 8UN, England

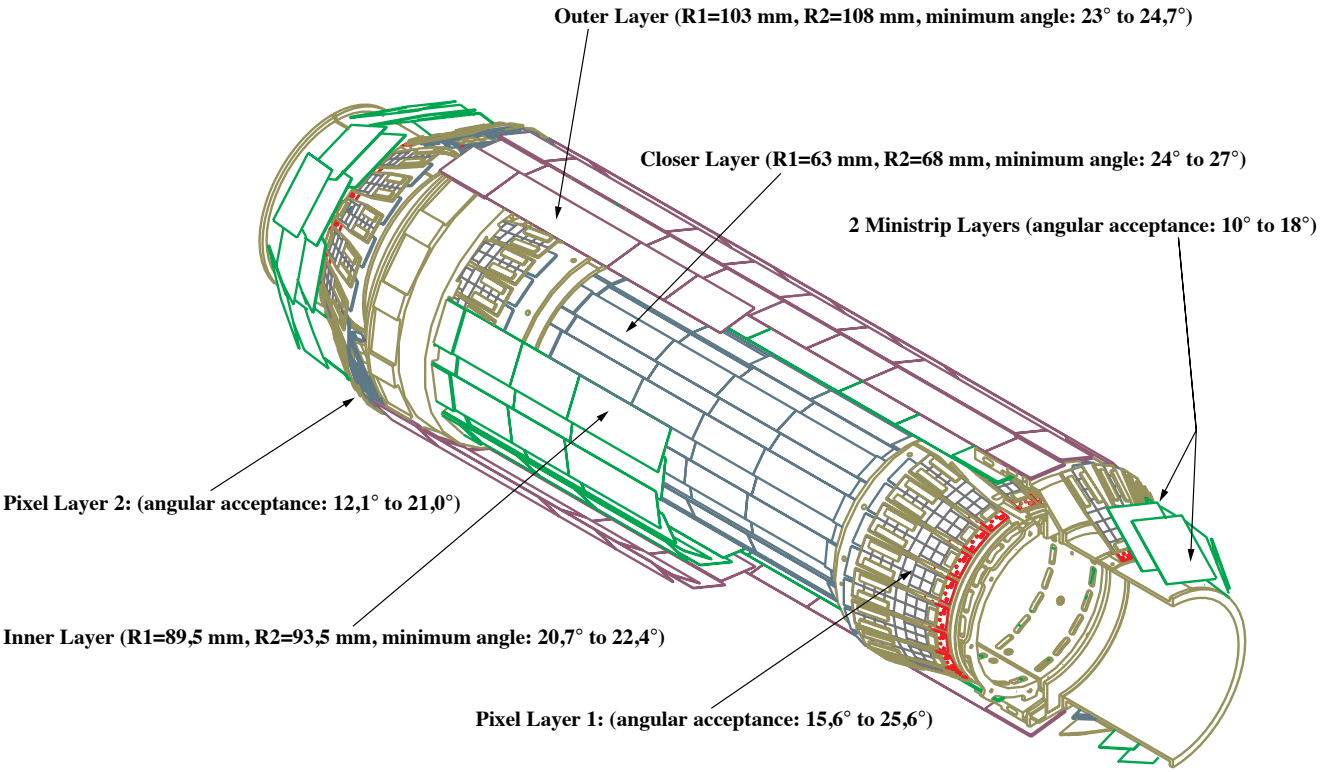

Figure 2: Layout of the DELPHI Silicon Tracker

new, and has a novel Rz measurement which is made with single sided detectors with p^+ implants, with the signals being routed to the ends of the detectors with a double metal technique. The diodes are either read out singly, or singly with one intermediate strip, or 'ganged' in pairs, with two connected intermediate strips, to give a choice of pitches, so the resolution can be optimised for tracks passing through at different theta angles. The Inner layer is built up of both double and single sided detectors, allowing the re-use of double-sided detectors from the previous vertex detector.

As discussed above, due to multiple scattering the resolution in the forward region is less critical. The pixel plaquettes are divided into ten regions of 24×24 pixels at large radius and six regions of 24×16 pixels at smaller radius. Pixels at the boundary between neighbouring chips have increased dimensions, so that blind regions in the active area are avoided. The ministrip plaquettes have a readout pitch of 200 μm with one intermediate strip.

4 Assembly into Modules and Crowns

The concept of the silicon tracker is modular: the plaquettes in each region are assembled into electrically independent modules or crowns, which are subsequently connected to their repeater electronics and mounted onto the support structure. The characteristics of these modules and crowns are summarised in table 2.

In the barrel the modules take the form of ladders of 4 or 8 modules, each forming two electrically independent halves. The front end electronics are mounted onto double sided BeO hybrids at each end of the modules, and kaptons join the hybrids to the repeaters. In

Characteristics of silicon plaquettes		Barrel				VFT	
		a	**b**	**c**	**d**	Pixels	Ministrips
supplier		Ham	SI	Ham	SI	CSEM	MICRON
single/double sided		ss	ss	ds	ds	ss	ss
double metal	p-side	no	yes	no	no	-	no
	n-side	-	-	yes	yes	-	-
length (cm)		5.99	5.99	5.75	6.07/7.91	6.9	5.3
width (cm)		3.35	3.35	3.35	2.08	$1.7 \rightarrow 2.2$	5.3
sensitive area(cm^2)		18.6	17.9	34.2	22.2/29.4	9.9	27.0
pitch (μm)	p-side	25	44	25	25	330x330	100
	n-side	-	-	42	49.5,99,150	-	-
readout pitch (μm)	p-side	50	44,88,176	50	50	330x330	200
	n-side	-	-	42,84	49.5,99,150	-	-
blocking strip	(n-side)	-	-	p^+	field plate	-	-
# readout channels		640	640	640x2	384x2	8064	256
wafer thickness (μm)		290	310	320	310	$290 \rightarrow 320$	300
implant width (μm)		8	8	12/14	6/8	-	60
biasing		FOX	Poly	FOX	Poly	DC	FOX
readout coupling		AC	AC	AC	AC	DC	AC
resistivity ($k\Omega$cm)		3-6	3-6	3-6	3-6	10	10
operating voltage (V)		60	60	65	60-95	40-60	60

Table 1: Characteristics of silicon plaquettes. There are 888 plaquettes in the full detector. The different types of plaquettes in the barrel, **a**, **b**,**c** and **d**, are arranged as shown in figure 3. Sensitive area counts $R\phi$ and Rz sides for cases of double sided detectors.

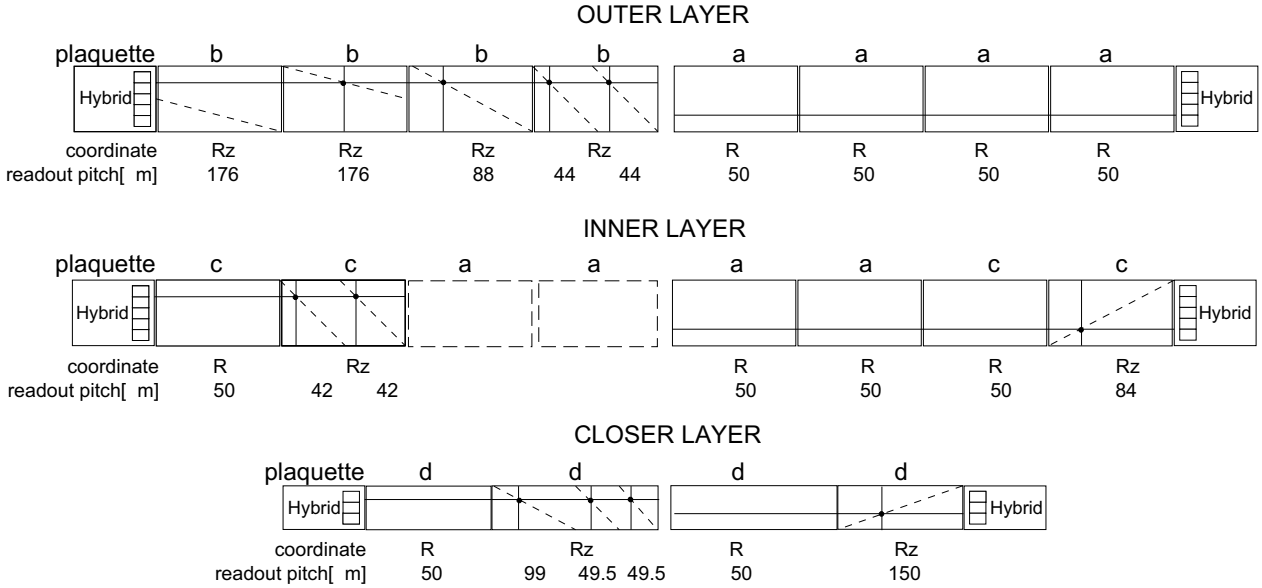

Figure 3: Arrangement of the detectors **a**,**b**, **c** and **d**, as defined in table 1, in the barrel. The left hand side of the figure illustrates the sides of the modules which face towards away from the beampipe, and the right hand side of the figure shows the sides of the modules which face towards the beampipe. A full technical description of the components of the barrel and the readout conventions can be found in [9] .

Characteristics of modules/crowns	Barrel			VFT		
	Outer	Inner	Closer	Pixel 1	Pixel 2	Ministrip
# plaquettes	16	8	4	19	19	12
sensitive area (cm^2)	292	208	103	189	189	324
dimensions (cm)	55.9x3.4	55.5x3.4	36.0x2.1	$r_{min} = 6.9$ $r_{max} = 8.4$	$r_{min} = 7.5$ $r_{max} = 11.2$	$r_{min} = 6.8$ $r_{max} = 11.2$
support material	kevlar + carbon	kevlar +carbon	kevlar +carbon	$\approx$ 2.5 mm Al crown	$\approx$ 3.5 mm Al crown	3 mm thick Al crown
chip choice	TRIPLEX	MX6	MX6	SP8	SP8	MX6
power/chip (W)	0.2	0.2	0.2	0.017	0.017	0.2
# chips	10	10	6	304	304	24
% overlap	15	13	12	37	12	15
rad tolerance (krad)	50	50	50	10	10	50
number	24	20	24	4	4	8
angle to z-axis (°)	0	0	0	12	32	49

Table 2: Characteristics of modules and crowns. Sensitive area counts $R\phi$ and Rz sides for cases of double sided detectors. The VFT detectors are supported on the crowns with ceramics in the case of the pixels, and aluminium plates in the case of the ministrips.

each quarter of the detector there is one repeater card per layer, serving 10 or 12 modules. Bond wires connect together the signal and bias lines between the detectors and hybrids. In the Inner layer this leads to one bias line connecting together diodes with polysilicon and FOXFET biasing, and this has operated successfully. For the Closer and Inner layers the electronic chip used is the MX6 [10], taken from the previous detector, and for the Outer layer the new TRIPLEX [11, 12] chip, with a noise performance of ENC $(283 + 17/\mathrm{pF})$. On the Rz side of this layer there is a small charge loss due to the combination of the double metal readout with intermediate strips [8] but the high S/N performance means that this leads to negligible loss in resolution. The use of double sided and back to back modules led to the choice of kevlar for the strengthening beams, with the addition of carbon fibre at the top of the beams to reduce the mechanical sensitivity to changes of humidity [13].

In the VFT, the pixel and ministrip plaquettes are mounted onto semicircular aluminium crowns, with inclinations with respect to the z axis of 12° and 32° for the pixel and 49° for the ministrip plaquettes. The electronics are connected to the repeaters with kaptons, with one repeater per crown for the ministrips and two repeaters per crown for the pixels.

The pixel plaquettes, each with 16 bump bonded chips [14], are arranged in groups of 19 onto each pixel crown. Bus lines bringing the data and control signals to each of the chips are integrated onto the detector substrate using a double metal process. This design reduces the amount of material and allows at the same time a reduction in the amount of signals by multiplexing on the integrated bus. On the other hand, it is a highly demanding design in terms of failure rate of the interconnection technique. The connection between the bus lines and the corresponding pad on the chip is achieved by the same bump bonding technique used for the pixel interconnection. The IBM C4 (Controlled Collapse Chip Connection) bump bonding process [15] was used, and a $(2.4 \pm 0.2) \times 10^{-4}$ failure rate was achieved. The remaining power busses are supplied via a flat kapton glued on top of the readout chips. On two cells per chip, a p well underneath the input pad defines a 30 fF calibration capacitance. Because of the large number of pixels and the expected low occupancy, a selective readout scheme was implemented on chip [16], identifying and outputting the addresses of the hit pixels. The connections between the detector substrate and the flat kapton, and then to the long kapton connected to the repeater electronics, are made with wire bonding.

The ministrip crowns each contain 6 pairs of back to back plaquettes. As for the barrel, MX6 chips were used, glued to 300 μm thick BeO hybrids. Due to the lack of space the hybrids are glued directly on top of the single sided plaquettes. A special ceramic or glass fan-in was used to match the 50 μm electronics pitch with the 200 μm readout one. The back to back detectors are rotated by 90° with respect to each other, to give a two dimensional readout. The implanted strips have an angle of 2° with respect to the edge of the detector, so by rotating modules in adjacent crowns a 4° stereo angle is created between the strips, helping the pattern recognition.

5 Readout Electronics

The repeaters are multilayer printed circuit boards mounted in the form of rows of semicircular discs at the ends of the Silicon Tracker. They contain buffers, control circuits and

power lines, and communicate with the readout systems in the barracks approximately 20m away.

The readout electronics of the barrel and ministrip parts of the Vertex Detector are similar enough to be steered and readout by a common system. At each second level DELPHI trigger 174080 analogue values are presented to the readout system corresponding to the same number of analogue channels sensing the barrel and ministrip parts of the Vertex Detector. This data is analysed in real time by an on-line computer farm made of 128 DSP56001 Digital Signal Processors. Each DSP is conveniently assigned to one, two or four detector modules and receives between 1280 and 1536 analogue readouts for the analysis. For every DSP the readout is performed in a serial form at the speed of 1 MHz. As all modules are read out in parallel thus it takes about 1.6 ms to read out the complete detector. Each DSP measures the pedestal and noise of every channel by averaging data over several events. The channels with significant signal are chosen, and signals on adjacent channels are correlated to match the typical charge spread patterns. The DSPs together with the digitization electronics are built into the FASTBUS modules named SIROCCO; two per module. The suppressed data is collected from these modules by a standard DELPHI readout processor and later it is joined to the common data stream. The effective suppression ratio achieved is in the order of 5/1000.

The 16 pixel repeaters are read out in parallel by the same number of FASTBUS readout units. The readout units themselves are read sequentially by a FASTBUS crate processor which combines the data stream. A custom designed card provides all necessary timing signals for the SP8 frontend chips [17]. The 16 front end chips of one plaquette are accessed sequentially and addressed separately one by one. This allows to the skipping of malfunctioning chips. With each second level trigger, the readout is started and all timing and clocking signals are activated. Due to the sparse data scan readout in the front end chips only the addresses of hit pixels are delivered to the plaquettes' data bus with a 5 MHz clock (1996: 1 MHz) and transfered to the crate processor. The total readout time for a full repeater with 160 frontend chips is typically 1.5 ms, including all bus transfer. The crate processor accesses a mask to suppress noisy pixels during acquisition time. This mask is set in advance using calibration run data and is updated with major changes in the detector settings. Online monitoring the pixel data spots new noisy pixels and writes them to a data base for later use. The suppression mechanism reduces the event size considerably. A typical event size from $\approx$ 1.2 million possible channels is up to a few hundred pixels per event during data taking conditions.

6 Mechanics

6.1 Mechanical Design

The principal challenges which had to be overcome for the mechanical design were as follows:

- Limited space available. The space constraints are provided by the 118 mm inner radius of the Inner Detector and the 56.5 mm external radius of the flange connecting the different sections of the beam pipe.
- The structure must be able to be installed inside DELPHI, which limits the total length of the detector to 1050 mm.

- Length of the detector and components. The Silicon tracker including the detectors and repeater electronics is 1033mm long. Within this there are modules which can be as long as 50 cm, mounted in parallel with much shorter modules. The mechanical design must be sufficiently rigid to support all components and suffer as little stress as possible from the varying deformations of the different components with changes of temperature, humidity, etc. At the same time, the extra support material must be kept to a minimum, so as to maintain the previous performance for the Rϕ impact parameter resolution in the barrel section.

- The mechanics must be able to reuse all double sided modules from the previous detector, and accommodate the design accordingly.

6.2 Support Structures

Figure 5 shows diagrammatically a cross section of the modules and supports between $z \approx 30$ cm and $z \approx 50$ cm. The barrel support consists of light aluminium endrings joined by carbon-honeycomb half cylinders [18]. The Inner and Outer layers are screwed to either side of this endring. The Closer layer has its own endring, which is connected to the barrel via an intermediate composite piece, which also serves to support the internal pixel layer. The thermal expansion coefficients between the components are matched as closely as possible to reduce mechanical stress [19]. The arrangement of the barrel detectors on the endrings is illustrated in figure 4. It can be seen that in order to fit into the space, the support beams on the Outer layer are glued to alternate sides of the modules. An adaptor piece connects the barrel to the forward cylinders. The forward cylinders support 3 crowns of VFT detectors, and also serve to route the kaptons towards the repeaters. The cabling of the repeaters is illustrated in figure 5. The cabling is arranged in such a manner that using a rotating jig it is possible to mount each section of the detector, together with its cabling and repeaters, sequentially on either side of the support cylinders. The resulting structure (see figure 6) maintains the material budget of the previous year in the barrel, and moves forward material to significantly lower theta than previously.

6.3 Cooling Considerations

The Silicon Tracker as a whole dissipates about 400W in an almost completely confined space. In order to remove the heat, a system of cooling with water at $20°C$ was chosen. The water is delivered to each section of the detector in 0.5 mm thick aluminium tubes with an internal diameter of 3.5 mm. The geometry of the cooling system is based upon mechanical considerations and the different power characteristics of each section. In the barrel, the greatest amount of power is developed in the Inner and Outer layers, which have a total of 880 0.2W chips. These layers are cooled with one tube per quarter. The shorter Closer layer is cooled in parallel, to avoid mechanical stresses due to temperature differences between the layers. The heat transfer between the cooling tubes and the hybrids is optimised with the use of heat paste [6] between all connections. Laboratory tests showed gradients of $4°C$ for the Inner and Outer hybrids, and a maximum of $6°C$ for the Closer layer, which has less contact with the endrings. For the pixel detectors, the power dissipation is about 40W, however the electronics are not localised on the hybrids

[6] supplied by SCHAFFNER, 5, Rue Michel Carre, 95100 Argenteuil, France

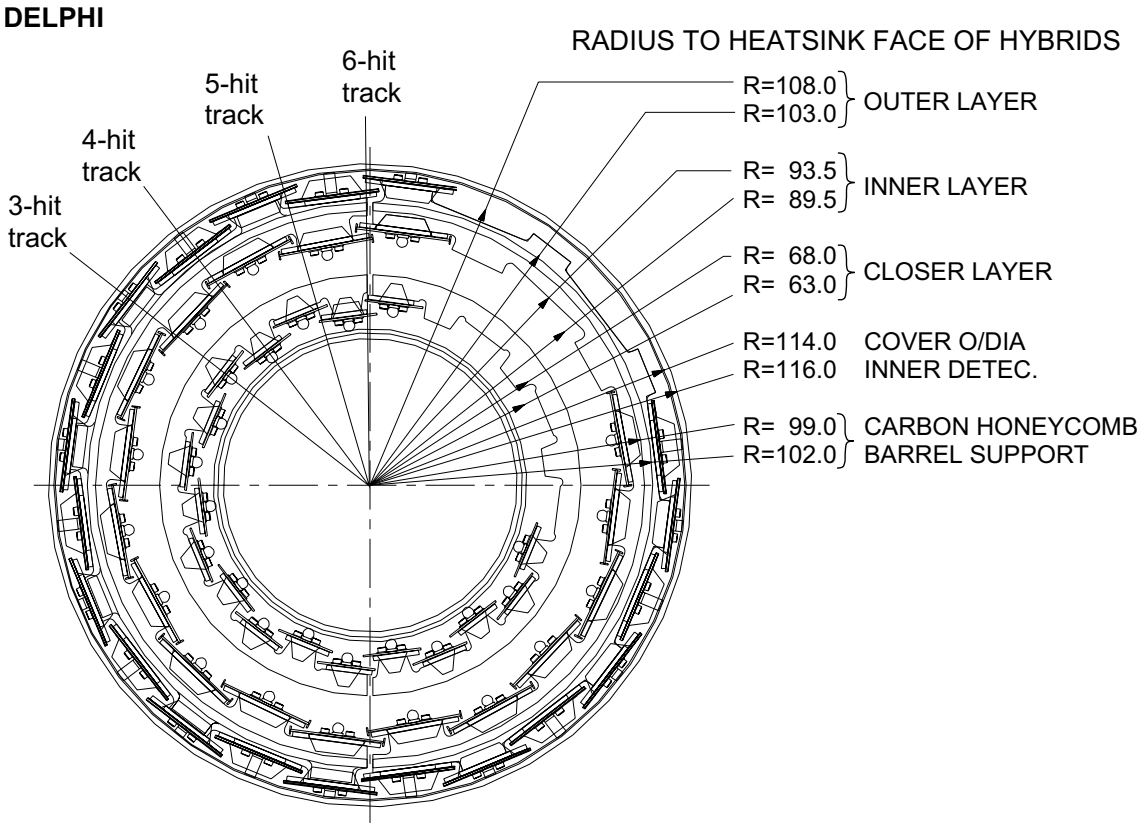

Figure 4: Cross section of the tracker showing the aluminium support rings of the Closer, Inner and Outer layers with the shape of the modules including the hybrids overlaid. There is a high degree of overlap in all layers, particularly the Outer layer which has roughly 15% overlap. The Inner layer has 20 modules only, as these modules come from the Outer layer of the old detector and previously formed a ring of 24 modules at higher radius. Spacers are screwed onto the Outer module hybrids to support the cover, which is made from 900 μm thick woven glass fibre with epoxy. The interior cover is supported with screws in 6 Closer layer hybrids. It is made from 1 mm thick Rohacel foam, with a 30 μm thick aluminium shield. The spheres used in the survey can be seen - these are removed before the installation into DELPHI. Note the overlaps between the top and bottom detectors, spanning the space where there is a gap in the support mechanics.

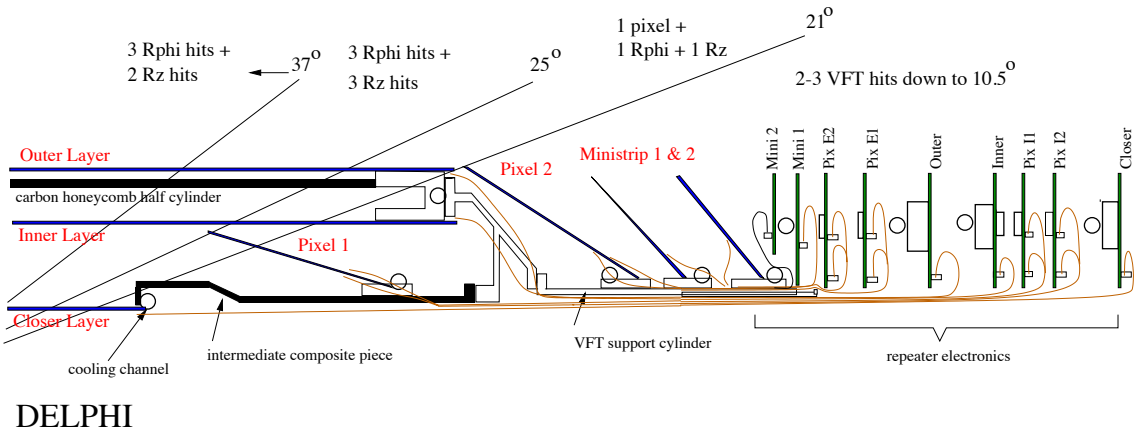

Figure 5: Cross section of the last 20 cm of detectors.

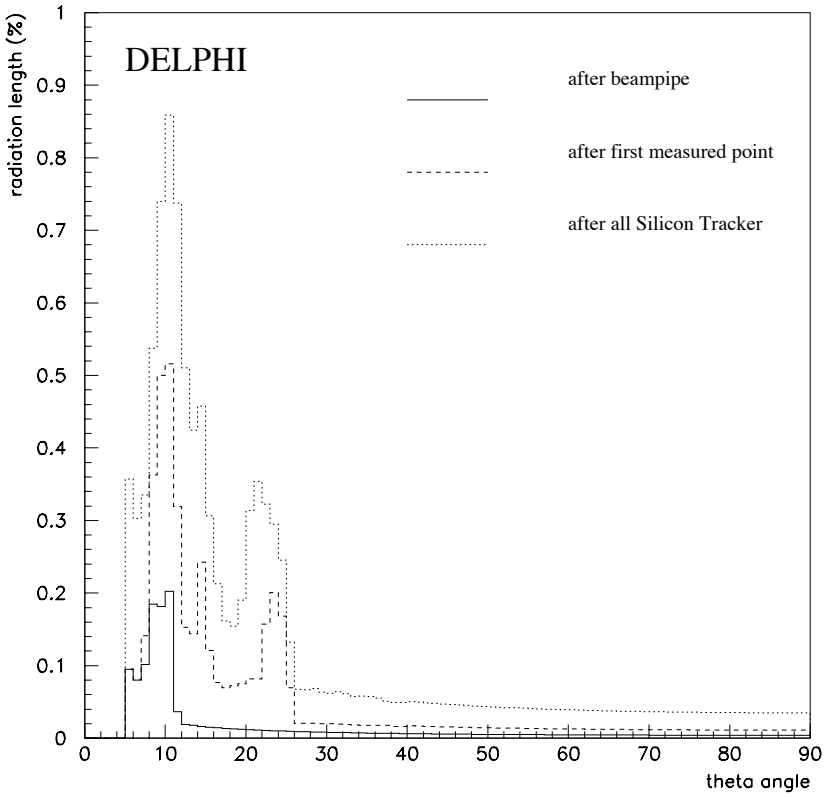

Figure 6: Material of the Silicon Tracker as seen by the particles traversing the detector at polar angles θ. The most important term for the impact parameter distribution is represented by the dashed line, which shows the material just after the first measured point. The values at $\theta = 90°$ are 0.4%, 1.1% and 2.7% for points after the beam pipe, the first measured point and the whole silicon tracker respectively.

but distributed over the detector. Here, the cooling functions by both conduction and convection, and the maximum gradients observed can be as high as $12°C$. The pixel and ministrip crowns are also cooled in parallel, as well as the repeater electronics, which are cooled with one tube per quarter looping through 5 or the 9 repeaters cards.

The cooling is operated on a siphoning principle, with the resultant underpressure protecting the detector from leaks in the system. The water pump used is driven by pressurised air, so there is no heat flow into the system, and the water is cooled by a system of fridges. Problems of algae developing have been avoided with the use of kemazur 1636 [7]. The system has a total of 20 independent cooling tubes, and bifurcation of the tubes inside the detector is avoided, except for short sections in the VFT crowns. This means that sections can be operated independently, and allows for a water flow of a total of 16 l/min.

6.4 Installation

The detector must be mounted inside DELPHI with the beam pipe already in place. The main weight of the detector is supported on carbon fibre rails via two aluminium skates per half shell. The skates are a maximum of 3 mm thick in order to pass between the barrel detectors and the second pixel layer, and widen to 8mm at the foot. At 90° there are also two side skate supports, made from 2mm thick aluminum, with a teflon coated head, which rests on side rails. Extra skates support the repeater electronics. In order to pass the support ring of the beampipe the rails are pulled apart, separating the two halves. The halves must be reassembled before entering the centre of DELPHI, which limits the total length of the detector to 1050mm. The detector is pulled into DELPHI with cords, and the two halves (each weighing around 3.5 kg) are brought together with a precision of 100 μm using locating pins mounted in the aluminium endring of the barrel. In order to study the problem, a complete mockup of the centre of DELPHI was built in the lab, and test insertions performed.

A photograph of part of the detector can be seen in figure 7.

7 Detector Performance

7.1 Real Time Control of the Detector

7.1.1 Operational Control

Stable and safe operation is a critical issue for the running of the Silicon Tracker. There is an automated response to changes in the data taking conditions or possible misbehaviours of the detector, running withing the framework of the general DELPHI slow controls system [24]. From the safety point of view the temperature of the detector is the most critical parameter. This is monitored with the use of 44 PT100 platinum thermometers [8], placed at the entry and exit of various parts of the cooling system. In the case of the Pixels some are mounted on the detectors themselves. The temperature variations seen on the inlet and outlet of the cooling are between $4°C$ and $7°C$ and are stable to less than $0.1°C$. Temperature variations are monitored in two independent ways. One monitoring system

[7] produced by Degremont-Erpac, France

[8] from MINCO Products Inc., Minneapolis, Minnesota, USA

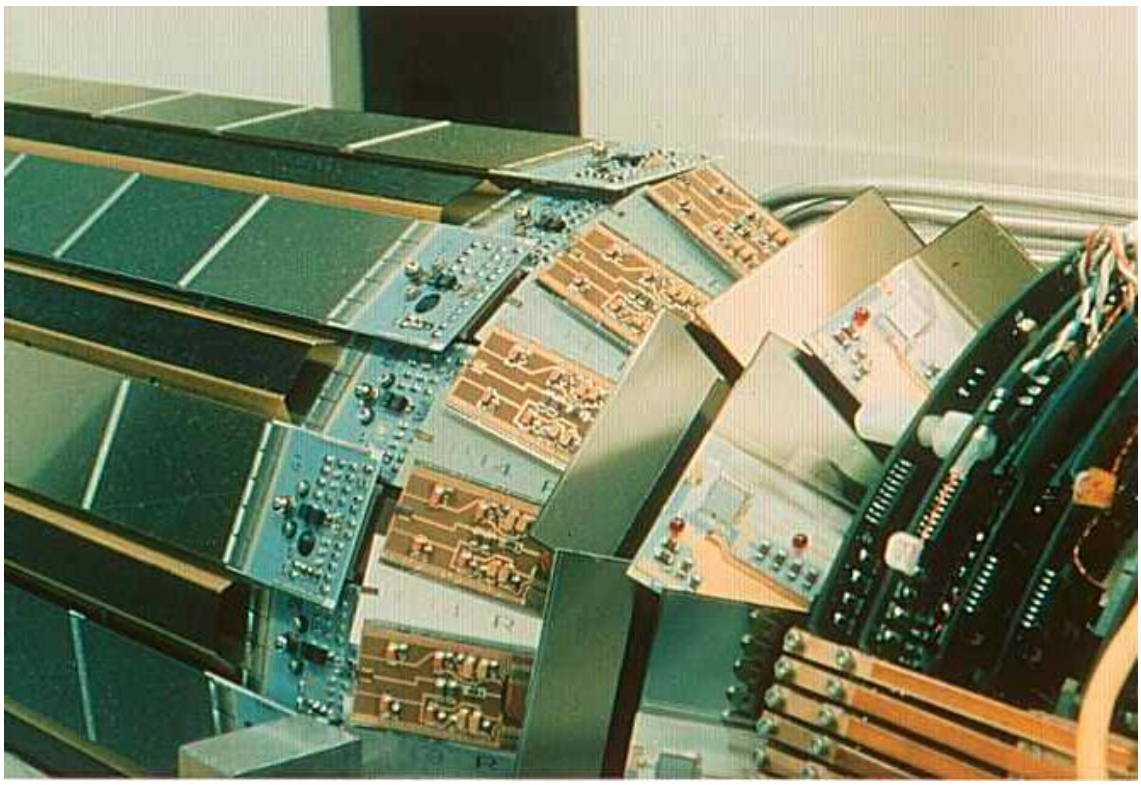

Figure 7: Photograph of part of the detector showing from left to right the Rz detectors of the Outer layer, the second Pixel plane, the two Ministrip planes and part of the repeater electronics.

records the values continuously, sends automatic calls to the experts if the temperature exceeds some warning levels and switches off the system if an alarm threshold is reached. The second one compares the thermometer levels with an hardwired threshold and is a backup in case of network/computer problems. Stable working temperature is essential for the alignment and daily checks are performed on the registered values.

Other parameters, such as bias voltages and currents, low voltages to electronic drivers and ambient humidity, are also monitored, and variations reported to experts. These parameters are also used in the subsequent data analysis to determine if the data collected for any specific detector are valid or not.

For the Pixels a more sophisticated controller supervises power supplies and threshold settings. A procedure was developed to detect and to react to an anomalous number of hit pixels, associated to either a high background or to a misbehaving chip. It is necessary to protect the detector against accidental very high occupancies because the power consumption of a cell connected to a hit pixel increases by a factor of about 10. If the required power exceeds the supply characteristics the detector may then trip off, leading to a jump in temperature of around $12°C$, and affecting badly the detector stability. A typical situation where this can arise is during the LEP injection, when the occupancy can be up to more than 2 orders of magnitude greater than the expected one in physics events. In addition, the threshold settings are crucial for the pixel efficiency (see section 7.2.2.) The thresholds are therefore adjusted automatically via a dialogue between the crate processor supervising the data acquisition and the detector control system supervising the power supplies and the threshold settings [20]. In addition, for the special period of LEP injection when the backgrounds are expected to be high, the discriminator thresholds are automatically raised. A stable operation has been obtained since the 1996 data taking.

7.1.2 Monitoring Data Quality

Online data quality checking is essential for debugging the detector after installation and for fast feedback during LEP physics conditions.

Within the DELPHI online cluster environment a standardized real-time data monitoring system has been developed[21]. A monitor program in the detector workstation spies and processes online the data from the detector acquisition system. Standard libraries are provided to access the detector data and LEP information. User routines contain the detector specific code to detect dead, noisy or inefficient modules.

The Silicon Tracker monitor program [22] reads the data stream of the entire detector. The subdetectors' data (Barrel, Pixels and Ministrips) are treated separately.

A simplified track search has been implemented for the Barrel detector. A quick online calculation of the residuals between tracks and hits gives information on the stability of the layers. For the pixel detector the modules' occupancy gives important information on the threshold settings and the quality of the crate processor suppression mask. New pixels to be masked from the readout are discovered online by the monitor program and written to a data base.

Trace plots document the development of several quantities in time. Two examples are given. Trace plot fig. 8 shows residuals as measured online in 1996 for the Outer layer of the Barrel detector. The LEP high energy periods at $\sqrt{s} = 161$ GeV/c^2 and 172 GeV/c^2 can be destinguished, separated by the summer break to install further cavities in LEP. During the autumn running less statistics were available. The information on the stability

of the detector is an essential tool for the decision whether several alignment periods are needed.

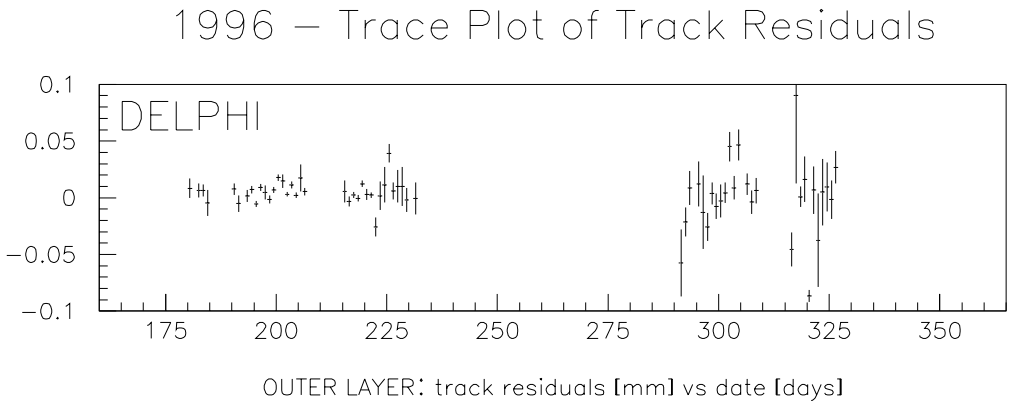

Figure 8: Trace plot of online calculated track residuals in the Outer layer of the Barrel detector.

Figure 9a shows day by day the integrated number of noisy pixels which were spot during the runs at $\sqrt{s} = 172\text{GeV/c}^2$ after the online masking in the crate processor. With the suppression mask unchanged, their number rises slightly in time. At the end of the high energy period, a new mask was applied. Suppression of these new noisy pixels reduces the event size considerably, as demonstrated in figure 9b and 9c for a run from November 13th, 1996.

7.2 Noise and Efficiency

7.2.1 Strip Detectors

Figure 10 gives a summary for the most probable signal over noise values for strip detectors shown as a function of the strip length seen by the amplifier. Due to the flipped modules on the Closer and the Inner layers one can distinguish, on each side of the module, between the $R\phi$ and z signals. Thus there are ten different values for the microstrip detectors of the Barrel part. The numbers given are normalized to values for tracks perpendicular to the detectors. For the Ministrip detectors of the VFT one overall value is given without correcting for track angles. One can see the very good performance of the Outer layer $R\phi$ detectors, which is due to a combination of the very low noise of the detectors and electronics. The highest value is measured for the Ministrip detectors, which have relatively short strips. Note that the strip length is only one of several sources of noise affecting the S/N level. Other sources could be interstrip capacitances depending on the detector pitches, detector current, capacitances between metal layers for the double-metal layer detectors, mode of supplying or charge loss effects from intermediate strips to the second metal layer. The noise performance of the detectors without n-sided readout is well described by an offset and a linear capacitance dependence taking into account

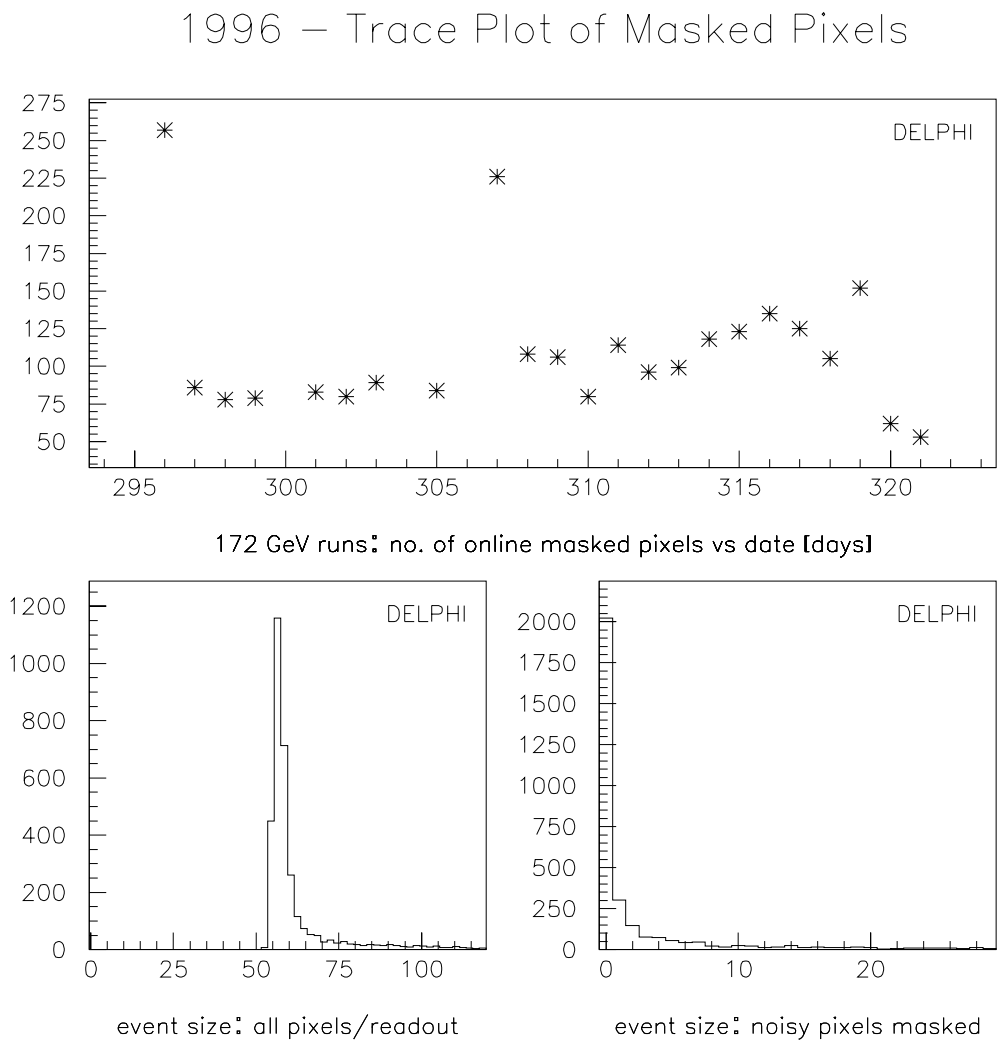

Figure 9: Trace plot of the number of online masked pixels. Suppression of these pixels reduces the pixel detector event size considerably. Blinking modules, recovering automatically from too high occupancy, lead occasionally to an increased number of noisy pixels. The mean event size after masking is 2-3 pixels, with the tail of the distribution coming from background with circulating beams.

the length of the strips and routing lines. The additional n implants cause an extra noise contribution dominating the other contributions (for other discussions see [8, 23]).

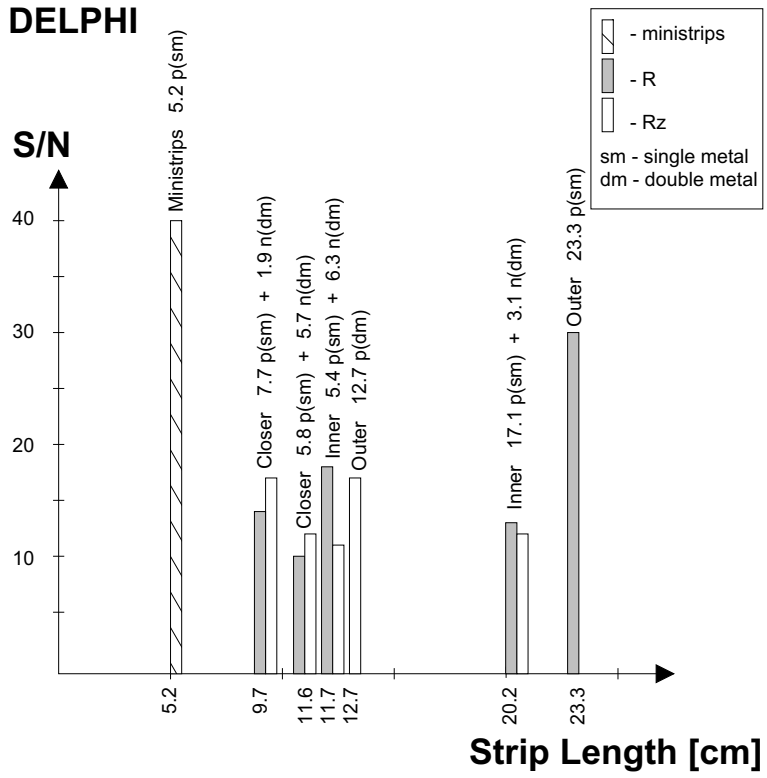

Figure 10: Signal over noise performance of the strip detectors. For each measurement the corresponding length of p and n strips connected to the amplifier is shown, and it is indicated if a double metal layer is used. The number shown is the most probable value of the S/N.

The efficiency of the Barrel part was studied using good quality tracks from hadronic events. The tracks were required to have a minimum momentum of 1 GeV/c, be reconstructed with a minimum number of track elements from other detectors, and lie within the polar angle range $27° < \theta < 153°$. Tracks with a hit in two layers were taken and extrapolated to the third layer, where a hit was searched for. An identical analysis was performed on a Monte Carlo sample simulated with a fully efficient vertex detector, and all results were normalised to this. Excluding dead and noisy detectors, the chance of finding the $R\phi$ hit associated with a track was found to be 93.5%, 98% and 99% for the Closer, Inner and Outer layers respectively. The problematic detectors made up a total of 10 %, 2% and 2 % in the three layers, and had a lower average efficiency of around 60%. For good impact parameter and momentum resolution a track should have a minimum of two associated $R\phi$ hits. The chance of this happening was measured to be 99.4%. The probability of finding the z hit associated with a track which has an $R\phi$ hit associated in the same layer was found to be 96% for the Closer layer and 98 % for the Outer Layer.

This analysis demonstrates the intrinsic silicon efficiency. When the Silicon Tracker is used in physics analyses the efficiency is slightly degraded due to S/N cuts requested by the physics teams, dead zones, and residual alignment problems. The degredation

depends on the stringency of the analysis performed, and varies between 2% and 4% for individual layers.

The efficiency for the ministrip part of the detector is studied using electrons from the dominant process of t-channel small angle Bhabha scattering. The scattered electron is tagged by the shower signature in the forward electromagnetic calorimeter. Due to the amount of material in front of this calorimeter at such θ angles most electrons give rise to electromagnetic showers before entering the tracking chambers. Hence no track reconstruction is required for selecting the Bhabha events. However, most of the electrons enter the VFT without showering in the relatively small amount of material of the beam pipe and Silicon Tracker support structures. These electrons are used to measure the hit efficiency in the ministrips. A set of 18000 Bhabha events was selected for the analysis using the information from the forward electromagnetic calorimeters. The reconstruction algorithm assigns ministrip points to the extrapolated track. A probability of 96.8% was found for registering at least one hit on the track. Excluding bad modules this number goes up to 99.3%.

7.2.2 Pixels

The detector efficiency is a function of two correlated parameters: the number of noisy pixels to be masked out and the discriminator threshold level, defining the minimum detected signal. The correlation between the two parameters is shown in fig. 11, integrated over the full detector in the final configuration; pixels were masked out if they responded to more than 1% of the triggers. According to this result, the detector can be safely operated setting the threshold in the (9000 : 10000) electron range, where the expected sensitivity to charged particles is above 99% and the number of masked pixels is at the 0.3% level. The leftover random noise, extremely important in a low redundancy tracking system, is measured to be at the part per million level.

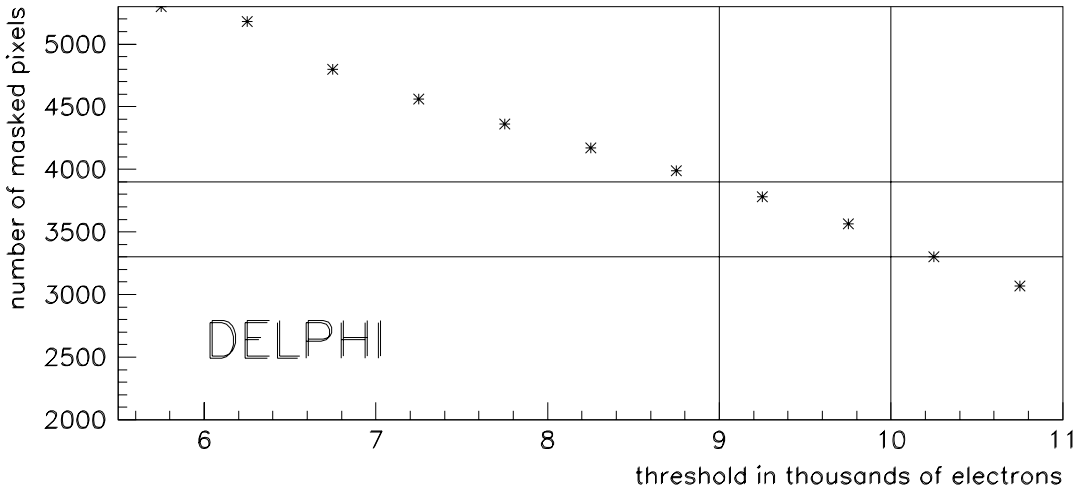

Figure 11: Number of masked pixels as a function of the discriminator threshold in the 1997 detector configuration.

The Pixel detector efficiency can be studied using tracks across the regions where neighbouring raquettes overlap. Tracks with an associated hit within 1 σ in the overlap region of one plaquette are extrapolated to the second plaquette, where a hit lying within 3 σ is searched for. Using this technique in the innermost Pixel crown, where neighbouring raquettes overlap by about 37%, efficiencies of the order of 95 % (see fig. 12) were measured.

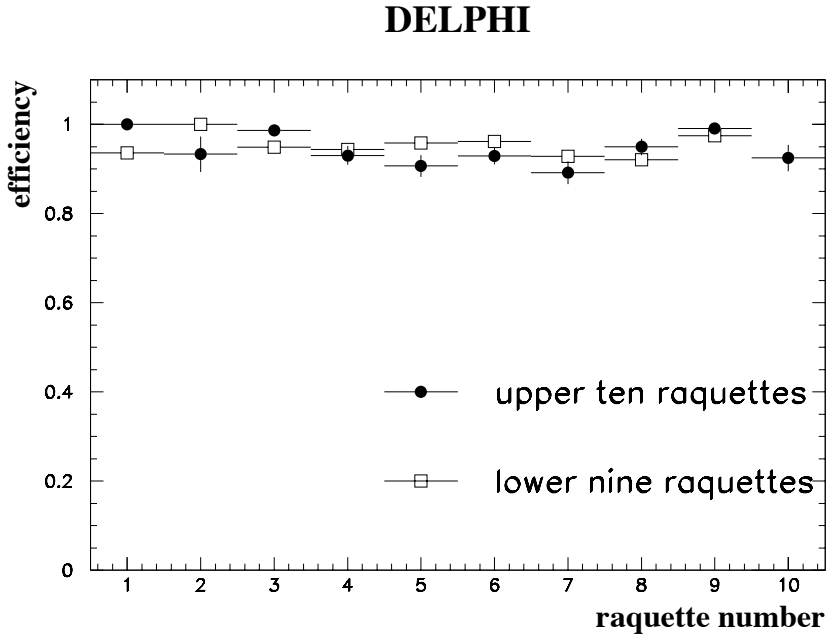

Figure 12: Efficiencies for the 19 Pixel raquettes in the upper and lower part of the crown which was fully equipped in 1996.

7.3 Alignment

The alignment of the full Silicon Tracker is performed in four steps.

The first one consists of an optical and mechanical survey of the individual components and of the whole structure of either half-shell. Being made before the insertion inside DELPHI, the survey gives no information on the relative position of the two half-shells. Also the geometry of either half-shell after insertion might slightly differ from the results of the survey, due to the lightness and small elasticity of the mechanical structure.

The second step begins after insertion. Cosmic tracks are then used to check for mistakes in the data handling, as well as for a rough prealignment of the two half-shells with respect to each other and to the other tracking detectors of DELPHI.

The last two steps, final alignment of the Barrel and of the VFT, begin immediately after the LEP start-up. Using tracks from e^+e^- collisions, the final alignment performs 4 tasks: parametrization and correction of the elastic deformations already mentioned, refinement of the survey for either half-shell, relative alignment of the two half-shells and external alignment of the whole Silicon Tracker. The alignment procedure for the Barrel

has already been described in detail [25] and more emphasis is put on the alignment procedure for the VFT.

7.3.1 Survey of the Silicon Tracker

The survey stage is different for the different detector components and it requires both optical and mechanical measurements. The procedure of the survey has already been described [27]; the differences due to the introduction of new module types and the extension to the VFT are stressed.

A major improvement was the implementation of a high precision 3D optical system [28] for the inspection of modules containing double sided detectors. Summarising, after their assembly, microstrip modules are individually measured by a camera [9] mounted on the same 3D machine [10] used for the mechanical survey. This measurement provides the position of all strips on a module with respect to two high precision reference spheres fitted on the opposite hybrids.

For double sided detectors used in the 94-95 version of the Vertex Detector, it was found the precision of the positioning of the masks on the n and p side of the detectors was consistent with the survey error. For the new Outer layer instead it was necessary to measure accurately the relative position of back to back detectors, which must be treated as two independent planes. This was accomplished by mounting on the measurement jig a reference sphere visible from the top and bottom part of the modules and using it to join the otherwise independent measurements of the $R\phi$ and z detectors. The same procedure is applied to Ministrip modules, for which the position of the single strips are referenced to two spheres that are glued to the ceramics of the module.

After assembling all modules into half-shells and half crowns, a 3D survey of detector planes and reference spheres is made with a high precision mechanical system, which provides the relative positions of all modules within one substructure.

Pixel detectors are first surveyed with a camera, before the bump bonding is done, determining the two-dimensional position of the chips with respect to the two external corners. These points are chosen because they are well defined and easy to access later. The wafer is bonded to the electronic chips into a single module and the kapton cable glued on top. The module is mounted on the support and its position, given by the location of the two corners plus the measurement of the module's plane, is related to that of three spheres mounted on the support. Very useful for cross checks, an additional measurement of the position of the two pins holding the ceramic support of each module is performed. The support is provided at the level of half shell and constitute one single unit then mounted on the mechanics of the Silicon Tracker.

Finally when VFT half crowns are joined to the Barrel support their relative position with respect to the half shell is measured.

The intrinsic accuracy of the survey is below 10 μm, but the overall precision of the description of the actual detector in DELPHI is limited by non rigid deformations induced by mechanical stresses. An overview of the mechanical structure suggests the easiest kind of distortions which can be induced are a twist of the Barrel around the z-axis, or a tilt of the Barrel endrings which maintains them parallel to each other (as the distance between the endrings is fixed by the module length). The presence of such coherent and non rigid

[9] Mondo Machine Developments Ltd., Leicester, UK.
[10] POLI S.p.A., Varallo Sesia, Italy.

deformations with amplitudes of few hundreds of microns was sometimes verified during the survey, while local deformations are below 25 μm.

The study of the actual non rigid distortion of the Silicon Tracker structure after insertion in DELPHI is performed with reconstructed tracks as described in the next sections.

7.3.2 Alignment of the Barrel

The four tasks of the alignment have already been mentioned: correction of the deformation due to insertion, refinement of the survey, relative alignment of the two half-shells and external alignment.

The procedure uses tracks from Z^0 decays: tracks of muon pairs, tracks from hadronic decays passing through the overlap regions of two adjacent modules and tracks from hadronic decays passing through only one module of each layer. For the first three tasks of the alignment the only information used from the other tracking detectors of DELPHI is the track momentum, in order to minimize the propagation of remaining distorsions from these detectors.

The most complex task is the internal alignment, together with the relative alignment of the two half-shells. Using the database from the survey as a starting point, tracks through overlaps allows one to align the Outer layer, muon pair tracks allow one to align the Closer layer with respect to the Outer one and the third sample of tracks allows one to align the Inner layer with respect to the other two layers. The actual procedure deals with 408 degrees of freedom and consists of a complex sequence of elementary steps repeated iteratively [25].

In addition to the deformations due to insertion one has to face a number of further complications:

- It has been found that individual modules might develop a small radial bending, not necessarily the same for all modules of a given layer. This effect is small for the Closer layer, but its amplitude might be as large as 150 μm in the middle of a module of Inner or Outer layer. It could be related to stresses induced during insertion and/or to humidity changes but is not fully understood yet. The radial bending can be measured using the overlaps between adjacent modules and is parametrized before internal alignment.

- A more fundamental effect should also be taken into account, namely the so-called "barycentric shift" that was observed in 1994 with the previous DELPHI Vertex Detector. It appears that the barycentre of the holes (and electrons) created by a particle crossing a detector and collected by the implant lines does not correspond exactly to the mid-plane of the detector. This effect is well established but still needs a detailed explanation [25, 26].

- One has also to take care of a possible and time or fill dependent acolinearity and momentum imbalance of the LEP beams when using muon pairs for alignment. Both effects are measured by the LEP machine group but they are not available in real time.

- Finally one has to cope with the much smaller integrated luminosity delivered by LEP2 at the Z^0 peak. In 1996 we collected only 400 muon pairs suitable for align-

ment. As a result of the limited statistics we have not yet reached the ultimate asymptotic impact parameter resolution. In the momentum interval relevant for B hadron decay products the effect is negligible. The lack of dimuon events can be partially compensated with the use of cosmic tracks.

As an illustration of what is gained by the internal alignment together with the correction of elastic deformations, we show in Fig. 13 the distribution of the residuals between the two hits of a track passing through the overlap of two adjacent modules, before and after internal alignment, for $R\phi$ hits and for z hits.

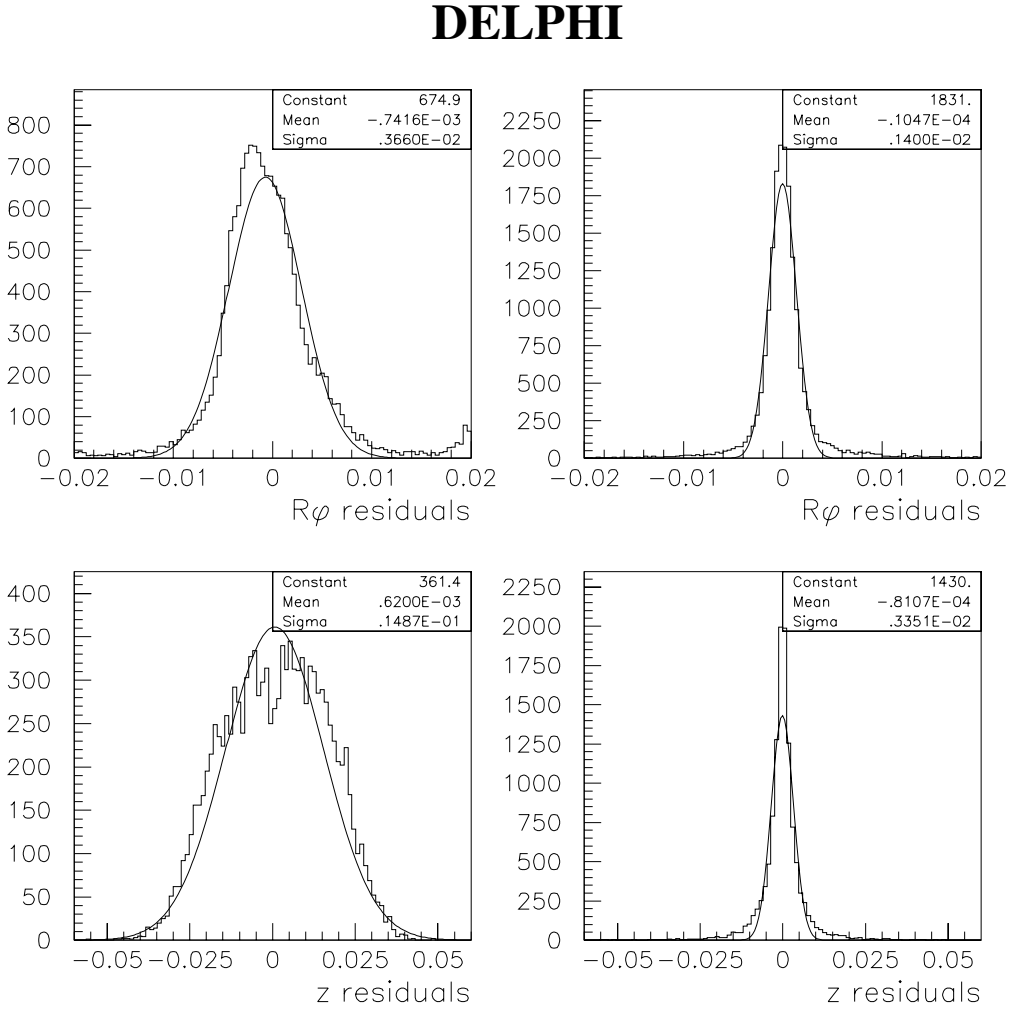

Figure 13: The residuals between two hits associated with tracks passing through the overlaps between modules. $R\phi$ residuals (upper plots) and z residuals (lower plots) are shown for the detector positions obtained from the survey (left side) and given by the final alignment (right side).

7.3.3 VFT Alignment

The VFT alignment procedure uses track elements already reconstructed with the use of the other tracking detectors. The procedure optimises the VFT module positions by minimising the χ^2 of tracks refitted over all track elements. In this way the correct weight is assigned to the different tracks, whose precision varies sharply with polar angle and with different combinations of tracking detectors. In addition, the precision of the VFT itself is exploited, as the improved precision of a track with associated VFT hits is taken into account, and overlapping detectors can be relatively aligned very precisely.

Proper functioning of the method requires correct hit association to the track, therefore if two or more hits from the same detector are within a window around the track, then these hits are not considered for the alignment, in order to avoid ambiguities.

In addition, the method must be statistically robust. In theory it is possible to include 6 degrees of freedom as free parameters in the fit, but due to the fact that the method uses as an input track elements from different track detectors, which may be not all sufficiently aligned, the χ^2 fit may have false local minima. To improve the robustness of the method the alignment is therefore done in several steps. The parameters are distinguished in order of their contribution to the alignment, in terms of the scale in which they are expected to move the single detectors. The global parameters at the level of each quarter and of single layers of the VFT are determined first, then the single module parameters are fitted in several steps. For example Pixel detectors are mechanically bound to the support only at one end and being long, thin and experiencing the pressure of the kapton cable, they can easily bend in polar angle; this affects the residual in the local Z coordinate being offset up to a few hundred microns. This local angle is therefore an important parameter to be measured and it is fitted at the early stages of the internal alignment.

An important factor in the alignment of the VFT is the overlap with the barrel Inner layer of the first Pixel layer, which occurs between $\theta = 20^\circ$ and $\theta = 25^\circ$. This provides a good link between the barrel and VFT for the alignment.

7.4 Alignment Performance

In the barrel, the precision of the alignment can be checked using residuals between overlapping modules, track hit residuals, and impact parameter distributions. The best hit precisions are found in the Outer layer, as these are used as constraints in the alignment procedure. The distributions are shown in figure 14 for the $R\phi$ and Rz projections. Taking the appropriate geometrical factor into account, the hit precision found is 9 μm, in the $R\phi$ projection and 11 μm for perpendicular tracks in the Rz projection. The Closer layer shows similar distributions with a hit precision of 11 μm in the $R\phi$ plane and 14 μm in Rz. The excess of these numbers over the Outer layer precision indicates the quality of the alignment. The Inner layer makes a less important contribution to the impact parameter resolution and is important mainly for pattern recognition. In $R\phi$ the hit precision is measured to be 13 μm and in Rz, measured at angles below 37° only, the precision varies between 70 μm and 90 μm.

An independent check of the alignment is provided by the impact parameter resolutions, displayed in figure 15. The top plot shows the impact parameter in $R\phi$ as a function of momentum, and is fitted with the function $28\ \mu\text{m} \oplus 71/(p\ \sin^{\frac{3}{2}}\theta)$, where p is the track momentum in GeV/c. The bottom plot shows the impact parameter resolution

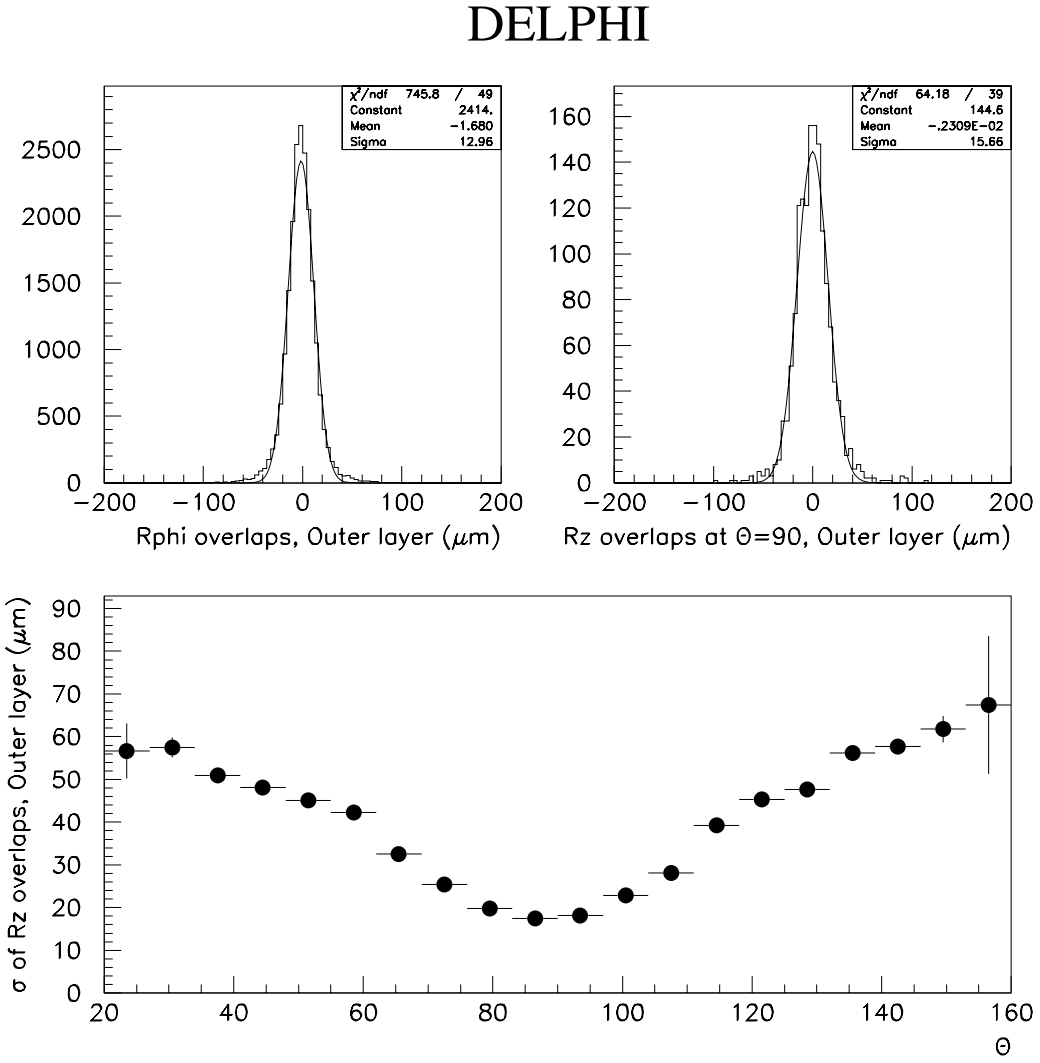

Figure 14: Residuals in overlapping detectors of the Outer layer in the $R\phi$ and Rz projections. The width must be divided by 1.41 to obtain the single hit precision. The Rz projection precision is also shown as a function of the polar angle θ.

in Rz for perpendicular tracks and is fitted with the function 34 μm $\oplus$ 69/p. In both these cases the first term is the asymptotic value and the second term contains the effects of multiple scattering. Taking into account the correct geometrical factors one estimates hit precisions of 8 μm and 9 μm in the two coordinates. The central plot combines tracks at all theta angles and fits the Rz impact parameter resolution with the function 39 μm $\oplus$ 75/(p $\sin^{\frac{5}{2}}\theta$).

The movements needed in the VFT for the global alignment are presented in figure 16, which shows the position of single detectors in the pixels and ministrips with respect to the prediction of the survey. The global alignment quality can also be demonstrated by forming residuals in $R\phi$ and $z_{\rm local}$ for the pixel detectors with respect to tracks fitted through the Inner layer of the Barrel (figure 17). Such tracks have a high precision and a a good extrapolation error to the pixel detector.

The internal alignment can be checked, as for the barrel, using overlaps. Figure 18 shows the residual in pixel overlaps. The internal hit precision derived from these plots is 100 μm.

8 Physics Performance

8.1 Performance of b-tagging in 1996 Run

Thanks to a good alignment for both $R\phi$ and z, and to the good performance of the reconstruction code, a high b-tagging efficiency [29] is obtained with the new vertex detector in 1996 both in the central region, 42°-132°, which was the acceptance of the previous VD for three layers, and in the new extended barrel region from 42° down to 25°.

In figure 19 the distribution of the impact parameter in real data for both $R\phi$ and z is shown in the two regions. The negative impact parameter distribution is displayed with the positive side. It is clearly visible that there is lifetime information also in the new extended barrel part.

In figure 20 the efficiency as a function of the cosine of the thrust's polar angle is given for b-tagged events. The full line is for the previous (up to 1995) microvertex detector which ended at θ= 42°, while the full points are for the new 1996 VD. A clear gain is visible in the new extended barrel region. In figure 21 the efficiency versus purity curves are given for the event tag in the barrel region defined by $|cos(\theta_{Thr})| < 0.7$, and in the extended barrel region defined by $0.7 < |cos(\theta_{Thr})| < 0.9$.

One of the main physics goal of LEP2 is the Higgs search. A good efficiency for the signal and a good background rejection can be reached at higher energy as shown in fig. 22, where the efficiency for an event tag over the full acceptance of the microvertex detector, i.e. $|cos(\theta)| \leq 0.9$ is shown for ZH, hA, WW events and the QCD background.

8.2 Improvement of Tracking in the VFT Region

The tracking situation in the forward region is considerably different to the barrel part of the silicon tracker. In the barrel the TPC [31] and the ID provide precise and high efficient tracking information. Here the emphasis is on high resolution tracking to provide b-tagging and vertexing information in $R\phi$ and z as discussed above. In the forward the TPC measures only the short track elements of particles leaving through its endcap. Additional tracking information is provided by the forward chambers before and after

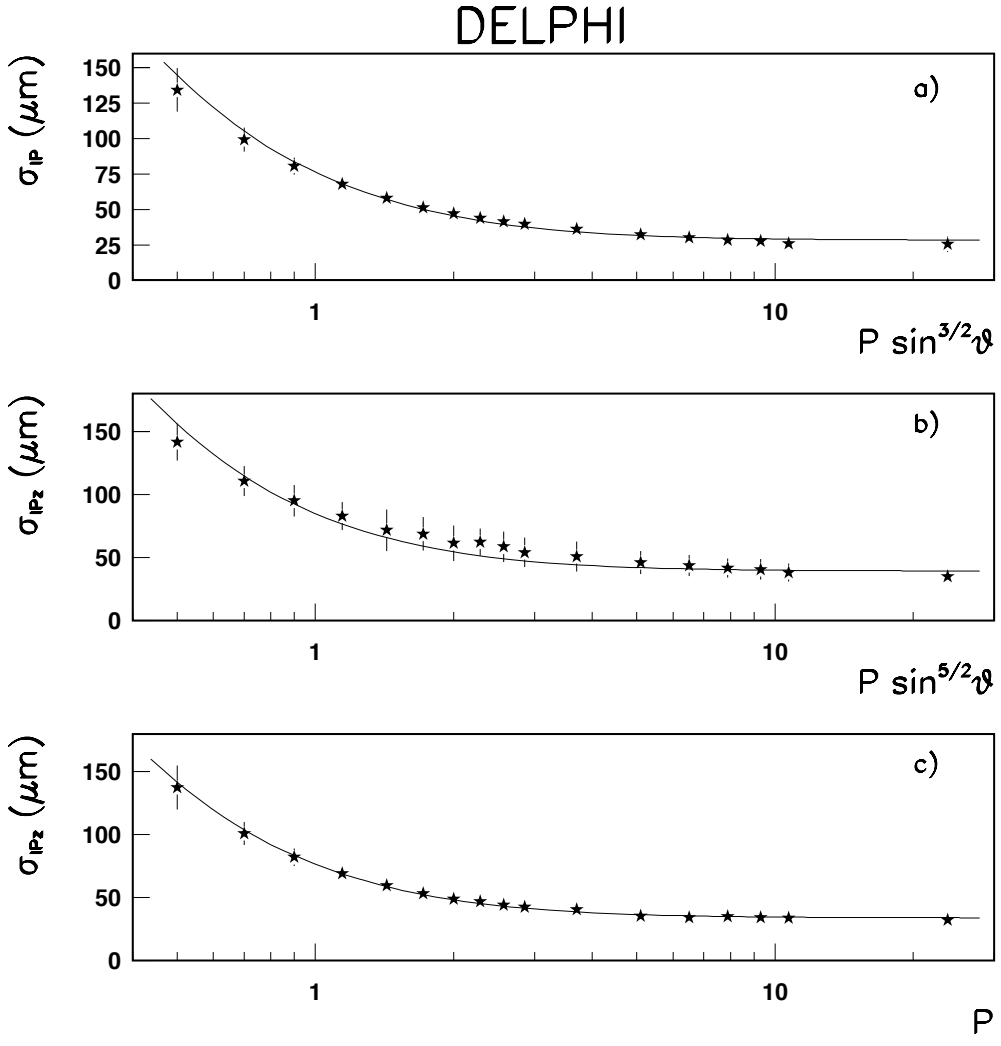

Figure 15: Impact parameter resolutions as a function of momentum, for: a) $R\phi$, b) Rz (all tracks), and c) Rz (perpendicular tracks) projections.

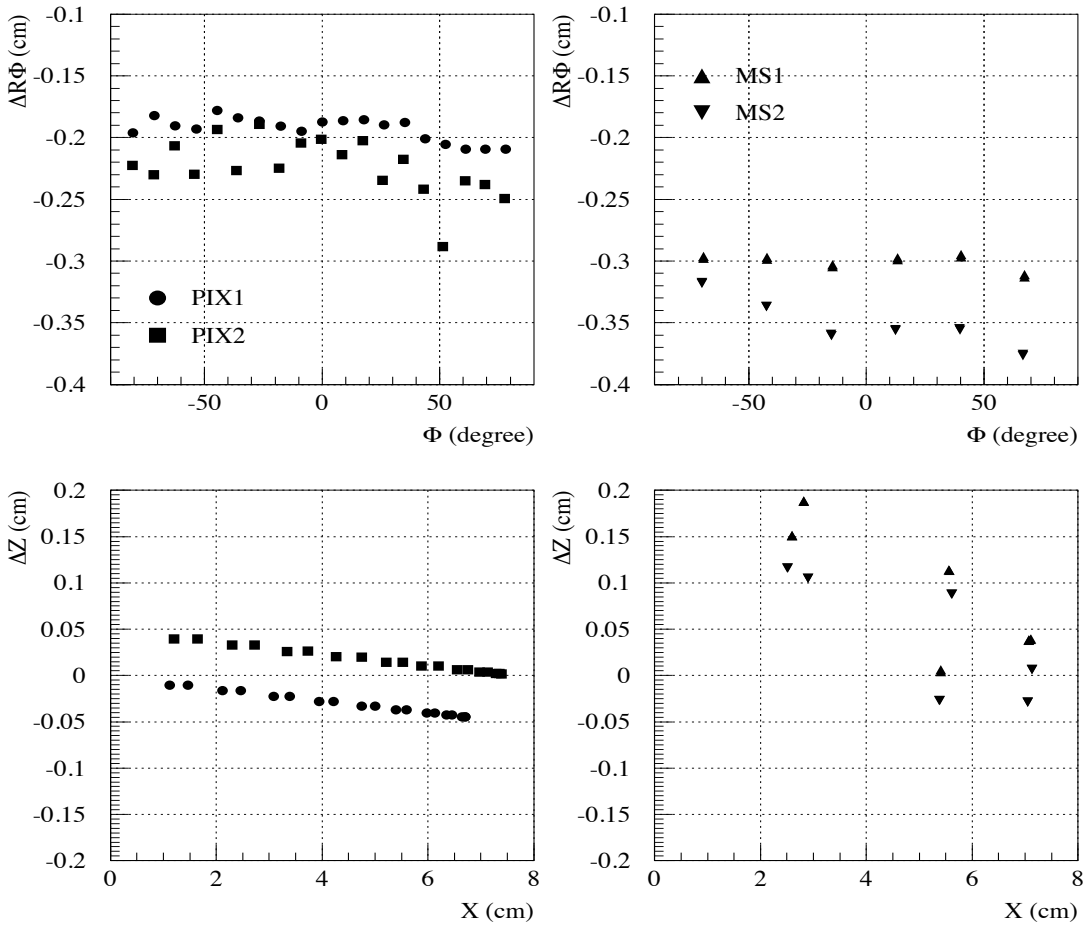

Figure 16: Differences between the survey and the final VFT alignment for the fully equipped quarter of 1996; the biggest movements found are a torsion of the structure, visible as an average $R\phi$ shifts depending on the z of the layers, and a tilt of the crowns w.r.t. the vertical axis, which shows up as a difference in z linearly dependent on x.

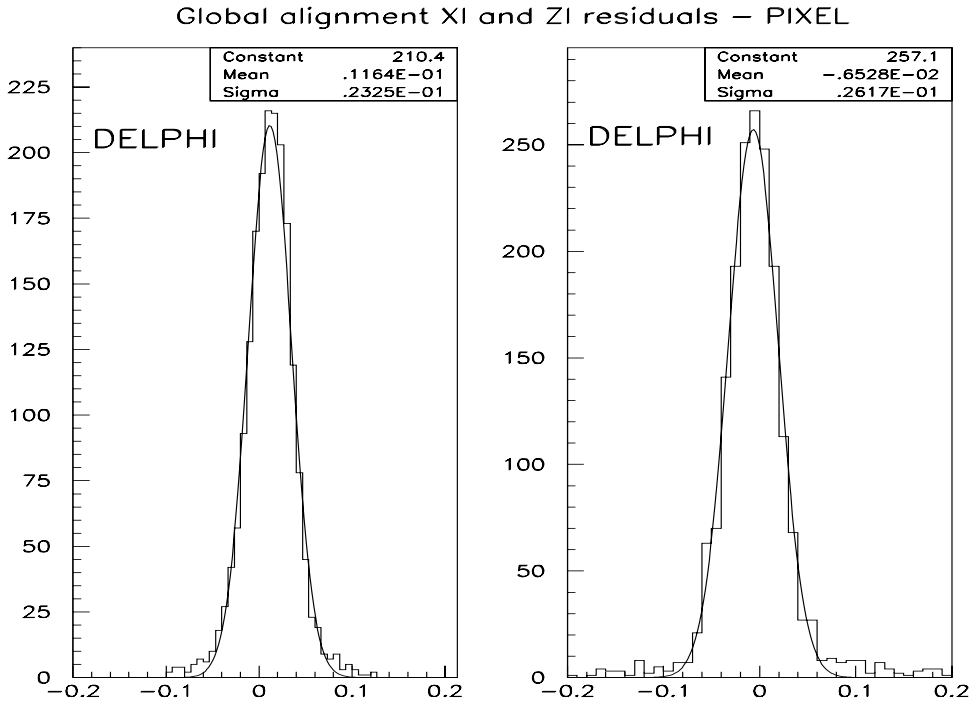

Figure 17: Global alignment residuals. The Rϕ and z_{local} residuals are shown in the left and right plot respectively.

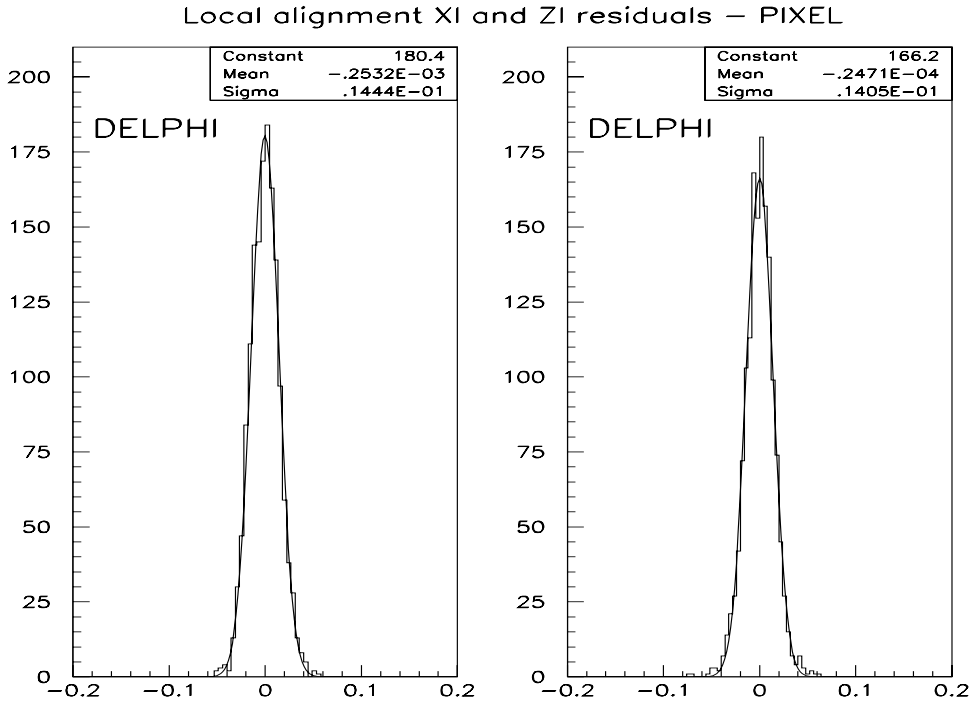

Figure 18: Local alignment residuals. The Rϕ and z_{local} residuals are shown in the left and right plot respectively

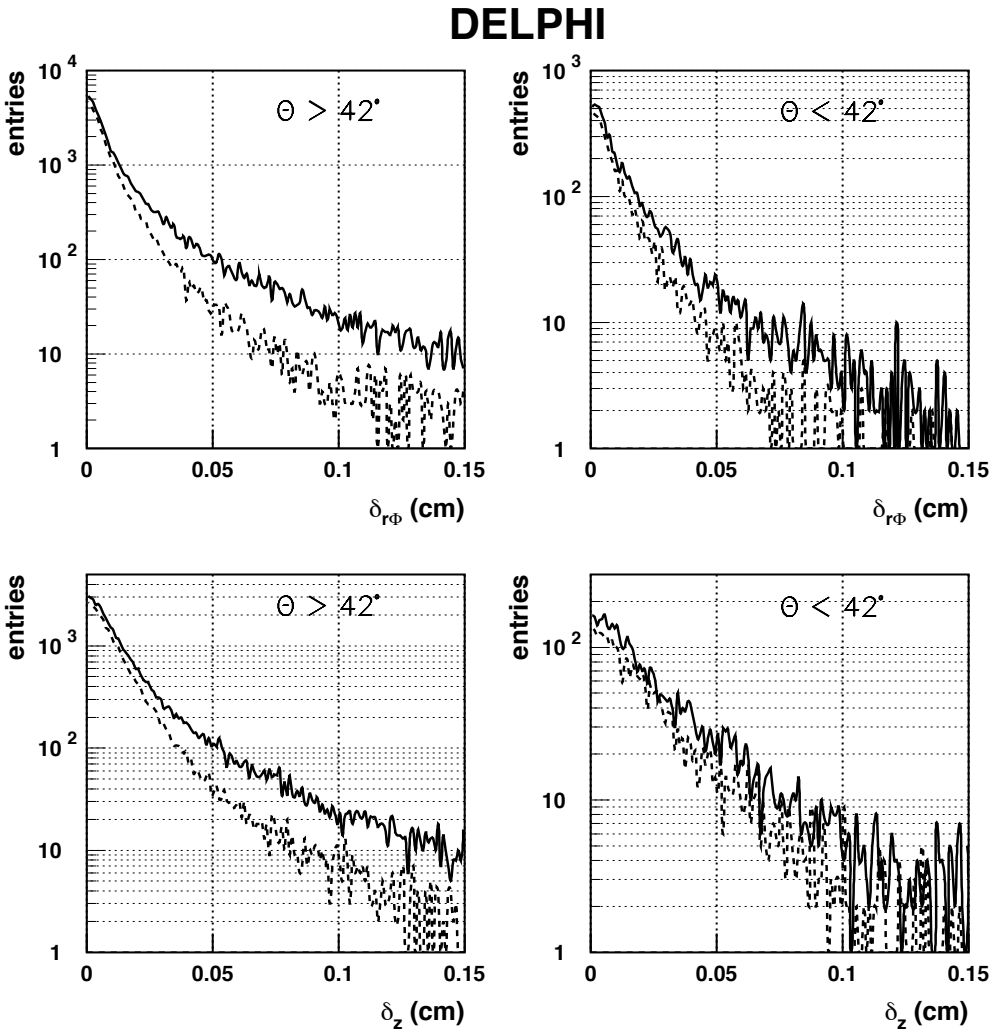

Figure 19: The impact parameter distributions for both $R\phi$ (upper) and z (lower) are shown in the Barrel (left) and forward (right) regions. The negative impact parameter distribution is superimposed on the positive distribution.

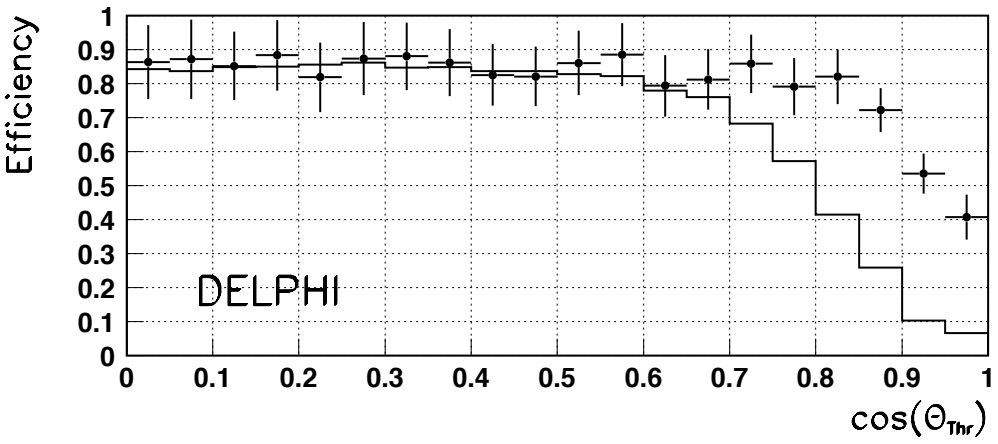

Figure 20: The efficiency versus $cos(\theta_{Thr})$ for the new microvertex detector (points) and the previous shorter one (full line).

the Forward RICH and by the measured track elements in the drift tube of the Forward RICH itself. Without the VFT the reconstruction efficiency is limited by interactions in the material in front of these detectors.

The VFT provides excellent measurements of space points with low backgrounds close to the beam pipe, especially the two pixel layers. This information is now fully integrated in the DELPHI Analysis Program. The VFT standalone pattern recognition is used to reconstruct track elements pointing to the primary vertex out of multiple hits in the different layers. These track elements are used in the global reconstruction as a seed for the track finding. To pick up the correct track elements in the other detectors the extrapolations are improved combining the VFT with the ID measurement or constraining the VFT track element to the primary vertex. Tracks reconstructed using the other detectors are improved adding the precise VFT hits.

For the simulation fig. 23 shows the improvement due to the VFT in the reconstruction efficiency of tracks in hadronic jets from particles coming directly from the primary interaction region having a momentum down to 0.5 GeV/c. For 91% of the particles crossing the VFT the hits are associcated to the tracks. The purity of the associations is 94%. This compare with 97.5% with a purity of 98% for the barrel silicon tracker. At 15° the tracks drop out of the acceptance of the ID giving rise to a lower acceptance. Special tracking algorithms are needed to make use of the hits in the VFT and in only one of the forward chambers.

9 Conclusions

The DELPHI Silicon Tracker, an ensemble of microstrips, ministrips and pixels, has been installed into DELPHI and is currently taking data. The Tracker is designed for the

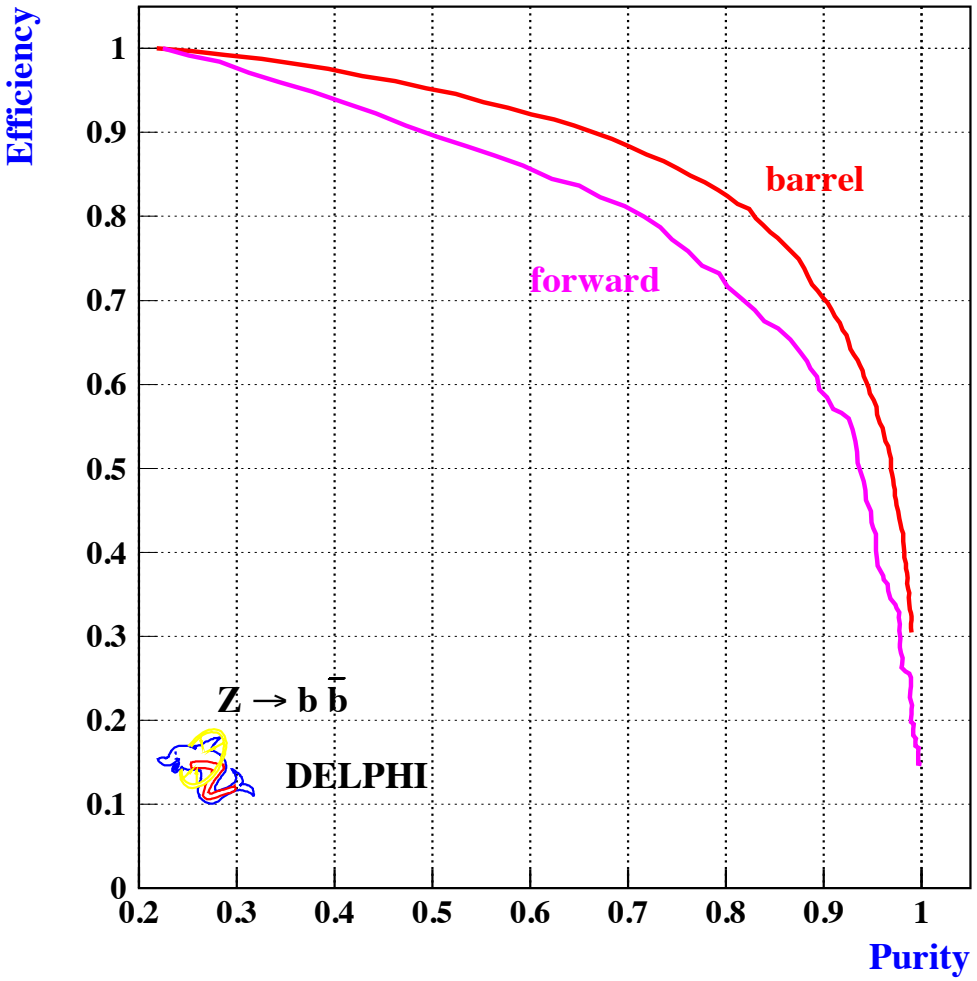

Figure 21: The efficiency versus purity curve for the event tag in the Barrel and in the forward region of the new microvertex detector. Here 'barrel' is defined as $\theta > 42^\circ$ and forward as $\theta < 42^\circ$

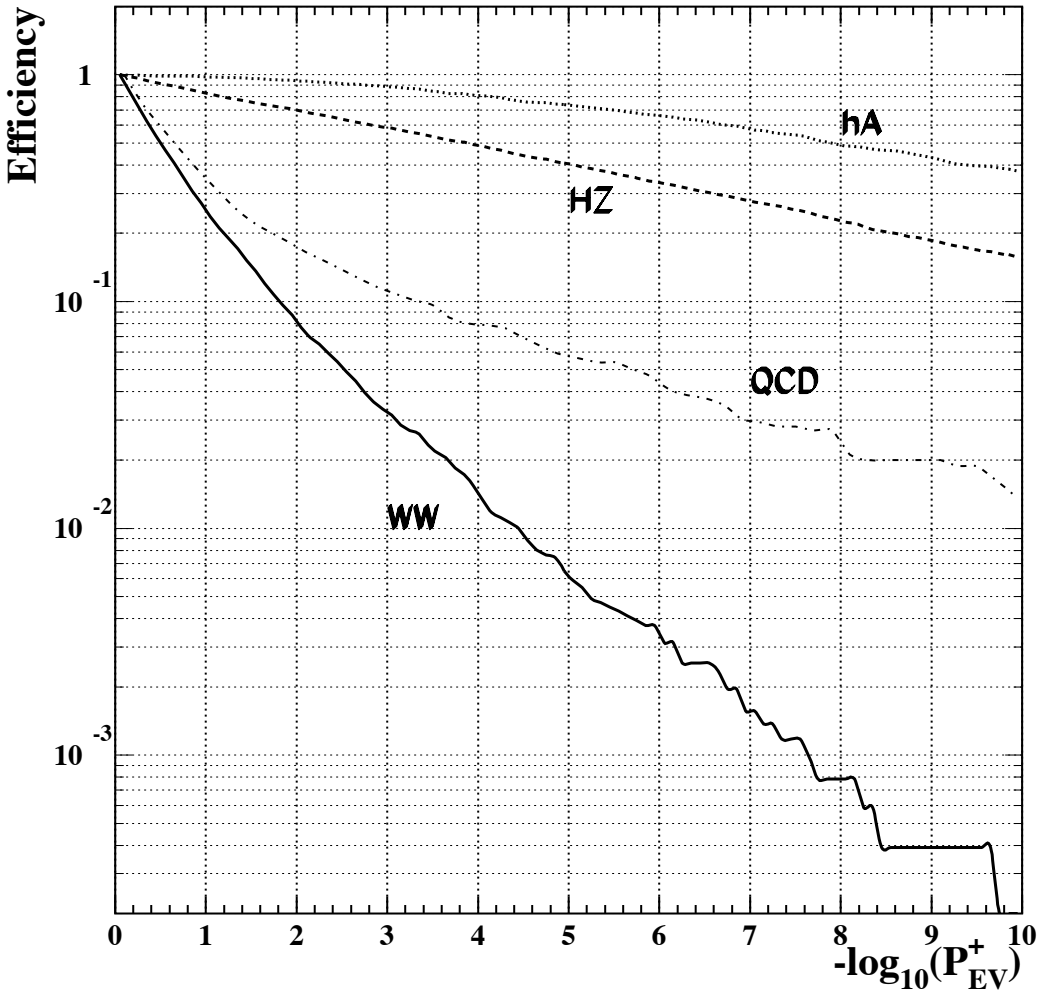

Figure 22: The efficiency for an event tag is shown for hA, ZH, WW events and the QCD background (taken from [30]).

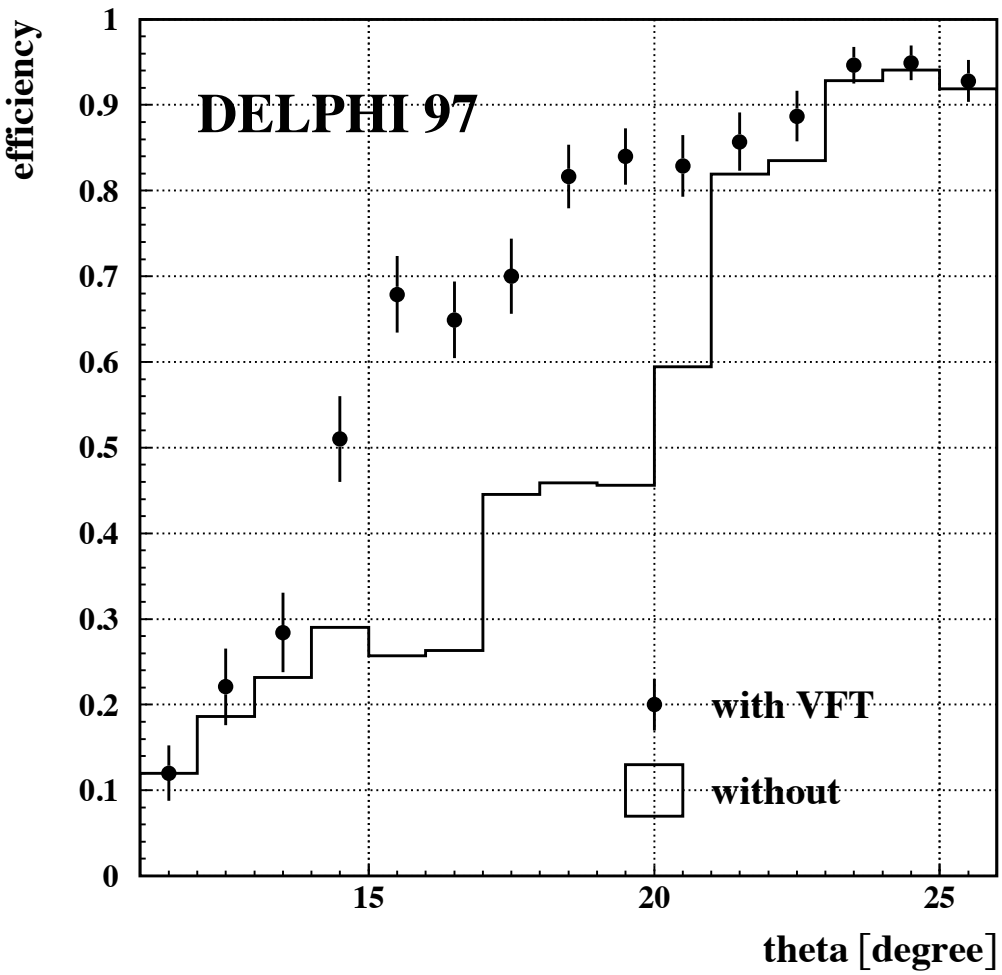

Figure 23: The reconstruction efficiency as a function of θ for tracks from particles coming directly from the primary interaction region having a momentum down to 0.5 GeV. The dots show the result for the 97 detector setup including the VFT. This can be compared with the efficiency removing the VFT from the tracking (line).

LEP2 physics programme. In the barrel part, asymptotic impact parameter resolutions of 28 μm in $R\phi$ and 34 μm in Rz have been measured. The amount of material has been kept low, and three dimensional b tagging information is available down to $\theta \approx 25°$. The resolution in Rz is optimised with the use of variable pitch detectors, and the Rz efficiency is kept high, with the use of both flipped modules and a p-side double metal readout. The forward part of the detector shows efficiencies of between 95% and 99 % in the pixels and ministrips, excellent signal-to-noise ratios of up to 40 in the ministrips, and noise levels at the part per million level in the pixels. Measurements of space points with low backgrounds are provided, leading to a vastly improved tracking in DELPHI below $\theta = 25°$.

Many parts of the Tracker are novel and were developped specially for the upgrade. At the same time the project was kept affordable with the careful reuse of components from the previous vertex detector. The Tracker has been operating successfully and equips DELPHI for physics analysis at LEP200.

Acknowledgements

The detector could only be constructed thanks to the dedicated effort of many technical collaborators in all laboratories participating in the project. We wish to express our appreciation to all of them and in particular to R. Boulter and A. Rudge.

The DELPHI Silicon Tracker Group

P. Chochula, P. Rosinský
Comenius University Bratislava, Faculty of Mathematics and Physics, Mlynskà dolina, SK-84215 Bratislava

A. Andreazza, G. Barker, E. Bravin, V. Chabaud, P. Collins, H. Dijkstra, Y. Dufour*, M. Elsing, P. Jałocha, Ch. Mariotti, K. Mönig, D. Treille, A. Zalewska
CERN, CH-1211, Geneva23, Switzerland

F.Ledroit
ISN Grenoble, Institut des Sciences Nucléaires, 53 Avenue des Martyrs, F-38026 Grenoble Cedex, France

C. Eklund, R. Orava, K. Österberg, H. Saarikko, R. Vuopionperä
Helsinki Institute of Physics, HIP and Department of Physics, University of Helsinki, P.O. Box 9, FIN-00014 Helsinki, Finland

W. de Boer, F. Hartmann, S. Heising, M. Kaiser, D. Knoblauch, G. Maehlum, M. Wielers
Inst. für Exper. Kernphysik - Universität Karlsruhe, Engesserstrasse 7, D-76128 Karlsruhe, Germany

P. Brückman,K. Gałuszka, T. Gdański,W. Kucewicz, J.Michałowski, H.Pałka
High Energy Physics Laboratory, Institute of Nuclear Physics, ul. Kawiory 26a, PL-30055 Kraków, Poland

V. Cindro, E. Križnič, D. Žontar
Univerza v Ljubljani, Institut Jozef Stefan, Jamova 39, P.O.B. 3000, SI-1001 Ljubljana, Slovenija

J.C. Clemens, M. Cohen-Solal, P. Delpierre, T. Mouthuy M. Raymond, D.Sauvage
CPPM Faculté des Sciences de Luminy, Université Aix Marseille II, 70 Route Léon Lachamp, F-13288 Marseille, France

M. Caccia, R. Campagnolo, F. Chignoli, R. Leoni, C. Meroni, M. Pindo, C. Troncon, G. Vegni
Dipartimento di Fisica, Università di Milano and INFN, Via Celoria 16, I-20133 Milano, Italy

F. Couchot, B. D'Almagne, F. Fulda, A. Trombini
Université de Paris-Sud, Lab. de l'Accelérateur Linéaire, IN2P3-CNRS, Bât. 200, F-91405 Orsay Cedex, France

J. Bibby, N. Demaria, P. Pattison, N. Vassilopoulos
Dept. of Nuclear Physics, Univ. of Oxford, Keble Road, Oxford OX1 3RH, UK

M. Mazzucato, A. Nomerotski, I. Stavitski
Dipartimento di Fisica, Università di Padova and INFN, Via Marzolo 8, I-35131 Padova, Italy

J.M. Brunet, B. Courty, G. Guglielmi, J.J. Jaeger, G. Tristram, J.P. Turlot
Collège de France, Lab. de Physique Corpusculaire, IN2P3-CNRS, F-75231 Paris Cedex 05, France

M. Baubillier, L. Roos, F. Rossel

LPNHE, IN2P3-CNRS, Universités Paris VI et VII, Tour 33 (RdC), 4 place Jussieu, F-75252 Paris Cedex 05, France

P. Sicho, V. Vrba, J. Masik
Institute of Physics, Academy of Sciences and Nuclear Center, Faculty of Mathematics and Physics, Charles University, Praha 8, Czech Republic

M. Bates, J .Bizzell, L. Denton, P. Phillips
Rutherford Appleton Lab., Chilton, Didcot OX11 OQX, UK

M. Gandelman, E. Polycarpo
Univ. Federal do Rio de Janeiro, C.P. 68528 Cidade Univ, Ilha do Fundão, BR-21945-970 Rio de Janeiro, Brazil

C. Bosio, V. Rykalin
INFN, Istituto Superiore di Sanità, Sezione Sanità, Viale Regina Elena 229, I-00161 Roma, Italy

C. Martinez-Rivero
Universidad de Cantabria, Facultad de Ciencias, C/Avda. Los Castros, S/N, E-39005 Santander, Spain

R. Brenner, O. Bystrom
ISV- Department of Radiation Sciences, University of Uppsala, P.O. Box 535, S-751 21 Uppsala, Sweden

W. Adam, N. Frischauf, M. Krammer, G. Leder, H. Pernegger, M. Pernicka, D. Rakoczy
Institut für Hochenenergiephysik, Oesterreichische Akademie der Wissenschaften, Nikolsdorfergasse 18, A-1050 Wien, Austria

K.H. Becks, J. Drees, P. Gerlach, K.W. Glitza, J.M. Heuser, S. Kersten, B. Überschär
Gesamthochschule Wuppertal Bergische Universität, Fachbereich Physik, Postfach 100127, Gausstrasse 20, D-42097 Wuppertal, Germany

* Yves was one of the driving forces during the design and construction of the Silicon Tracker. He was killed in an avalanche on the Pointe Percée in January 1996, a victim of his passion for the high mountains. We would like to dedicate this paper to his memory.

References

[1] The DELPHI Collaboration, *Proposal for the upgrade of DELPHI in the Forward Region*, CERN/LEPC/92-13/P2 Add2, 16th October 1992.

[2] V.Chabaud et al., *The DELPHI silicon strip microvertex detector with double sided readout*, Nucl. Instr. and Meth. **A368** (1996) 314.

[3] N.Bingefors et al., *The DELPHI Microvertex detector*, Nucl. Instr. and Meth. **A328** (1993) 447.

[4] R.Brenner: *The upgrade of the Vertex Detector to form the central part of the Silicon Tracker in DELPHI*, Nucl. Instr. and Meth. **A386** (1997) 6.
V.Chabaud: *The DELPHI Silicon Tracker - Barrel part*, to be published in the Proceedings of the 5th International Conference on Advanced Technology and Particle Physics, Como, Italy, 7-11 October 1996.

[5] A.Andreazza et al., *The DELPHI Very Forward Tracker for LEP200*, Nucl. Instr. and Meth. **A367** (1995) 198.
Ch.Meroni, *The forward extension of the DELPHI Silicon Tracker*, Proceedings of the fourth International Workshop on Vertex Detectors, June 1995, Ein Gedi Resort, Dead Sea, Israel, p.29.

[6] D.Sauvage et al., *A Pixel Detector for the '95 Upgrade of the DELPHI Micro Vertex Detector*, CPPM - 95-05 and Proceedings of the fourth International Workshop on Vertex Detectors, June 1995, Ein Gedi Resort, Dead Sea, Israel, p. 53.
K.H.Becks et al., *Progress in the construction of the DELPHI pixel detector*, to be published in the proceedings of the III International Workshop on Semiconductor Pixel Detectors for Particles and X-rays, March 24-27, 1996, Bari, Italy.
K.H.Becks et al., *The DELPHI pixels* , Nucl. Instr. and Meth. **A386** (1997) 11.

[7] V.Cindro et al., *The design of silicon ministrip detectors for the DELPHI Very Forward Tracker*, Nucl. Phys. B (Proc. Suppl.) **44** (1995) 292.
M.Krammer, *The construction of the DELPHI Very Forward Ministrip Detectors*, Proceedings of the fourth International Workshop on Vertex Detectors, June 1995, Ein Gedi Resort, Dead Sea, Israel, p. 41.
W.Adam et al., *The status of the DELPHI very forward ministrip detector*, Nucl. Instr. and Meth. **A 379** (1996) 401.
W.Adam: *Performance of the DELPHI VFT ministrip detectors*, to be published in the Proceedings of the 5th International Conference on Advanced Technology and Particle Physics, Como, Italy, 7-11 October 1996.

[8] I. Stavitski, *DELPHI vertex detector in 1996*, presented at conference "Frontier detectors for frontier physics", 26-30 May, 1997, Biodola, Italy
P.Collins, *Experience with silicon detectors at the DELPHI experiment, LEP*, Nucl. Instr. and Meth. **A383** (1996) 1.

[9] A. Zalewska, *Conventions for the barrel part of the Delphi Silicon Tracker 1996* , DELPHI note 96–146 MVTX 18, 24 October 1996.

[10] P. Seller et al., Nucl. Instr. and Meth. **A214** (1992) 393.

[11] J.Ardelean et al., *TRIPLEX: An Amplification and Trigger Chip for a Si-strip Microvertex Detector*, internal note of LAL, Orsay.

[12] R.Brenner, C.Eklund, *First Testbench Measurements of the DELPHI Vertex Detector Outer Layer Modules for the 1996 Upgrade*, HU-SEFT RD 1995-04.

[13] P.Collins, *The Alignment and Performance of the DELPHI Double Sided Vertex Detector*, Proceedings of the fourth International Workshop on Vertex Detectors, June 1995, Ein Gedi Resort, Dead Sea, Israel, p. 13.

[14] M. Cohen-Solal and J.C. Clemens, *Electronics for pixel detectors*, Proceedings of the 9^{th} International workshop on room temperature semiconductor X and γ ray detectors, associated electronics and applications, Grenoble, France, September 1995, Nucl. Instr. and Meth. A380 (1996) 335.

[15] L.F. Miller, *Controlled Collapse reflow chip joining*, IBM J. of Res. and Dev. 13, no.3 (1969), 239-250.

[16] J.J. Jaeger et al., *A sparse data scan circuit for pixel detector readout*, IEEE Trans. Nucl. Sc. 41, no.3 (1994), 632-636.

[17] C. Aubret, J.M. Brunet, B. Courty, L. Guglielmi, G. Tristram, J.P. Turlot, *DELPHI Pixel Detector Readout*, Collège de France, Paris, September 13, 1996, available via WWW:
http : *//cdfinfo.in2p3.fr/Experiences/Delphi/VFT/vft.html*

[18] L. Denton, *Distortion Tests made on the DELPHI Barrel Support*, internal RAL memorandum, 8th March 1995.

[19] M.Raymond et al., *Design and manufacture of an accurate composite piece*, CERN 94-07, Proceedings of the International Workshop on Advanced Materials for High Precision Detectors, pages 179-187.

[20] S. Kersten, *Slow Control for the DELPHI Pixel Detector*, University of Wuppertal, May 9, 1997, available via WWW:
http : *//www.uni − wuppertal.de/FB8/groups/Drees/detlab/vft_slowctrl.html*

[21] V.Chorowicz, *The real-time monitoring in DELPHI*, Delphi note 95–30 DAS 163, March 6, 1995.

[22] J.M.Heuser, M. Caccia, L. Roos, *Online monitoring of the DELPHI VFT pixel detector*, DELPHI note 96–150 MVX 19, October 24, 1996

[23] M. Krammer, H. Pernegger, *Signal collection and position reconstruction of silicon strip detectors with 200 μm readout pitch*, HEPHY–PUB–648–96
C. Troncon, *Measurement of spatial resolution and charge collection in double sided double metal silicon microstrip detectors* Nucl. Phys. Proc. Suppl. 44 , 287–291, 1995
P. Seller et al. *Noise in detectors and readout circuits*, RAL TR 96–001.

[24] T.J.Adye et al.
The design and Operation of the Slow Controls for the DELPHI experiment at LEP
Nucl. Intrum. and Methods A349 (1994), 160-182.

[25] V.Chabaud, A.Andreazza, P.Collins, H.Dijkstra, *Alignment of the DELPHI vertex detector*, DELPHI note 95–177 MVX 10, December 1995.

[26] A.S. Moszczyński, *The Barycentric Effect in Semiconductor Position Sensitive Detectors*, REPORT No. 1749/PH, Institute of Nuclear Physics, Cracow.

[27] A. Andreazza et al., Nucl. Instr. and Meth., A312 (1992) 431.

[28] S. Testa, Tesi di Laurea in Fisica, Università degli Studi di Milano, Milano, luglio 1993.
E. Bravin, Tesi di Laurea in Ingegneria, Politecnico di Milano, Milano, dicembre 1995.

[29] G.Borisov and C.Mariotti, *Performance of b-tagging in DELPHI at LEP2*, preprint CEN SACALY DAPNIA/SPP-97-06 and INFN-ISS 97/3, April 1997.

[30] P. Abreu et al., (DELPHI Collaboration), *Search for neutral and charged Higgs bosons in e^+e^- collisions at $\sqrt{s} = 161$GeV and* 172GeV, submitted to Zeit. Phys. C.

[31] P. Abreu et al., (DELPHI Collaboration), *Performance of the DELPHI Detector*, Nucl. Instr. and Meth. **A378** (1996) 57.